Superconducting TESLA cavities

B. Aune,[1] R. Bandelmann,[4] D. Bloess,[2] B. Bonin,[1,*] A. Bosotti,[7] M. Champion,[5] C. Crawford,[5] G. Deppe,[4] B. Dwersteg,[4] D. A. Edwards,[4,5] H. T. Edwards,[4,5] M. Ferrario,[6] M. Fouaidy,[9] P.-D. Gall,[4] A. Gamp,[4] A. Gössel,[4] J. Graber,[4,†] D. Hubert,[4] M. Hüning,[4] M. Juillard,[1] T. Junquera,[9] H. Kaiser,[4] G. Kreps,[4] M. Kuchnir,[5] R. Lange,[4] M. Leenen,[4] M. Liepe,[4] L. Lilje,[4] A. Matheisen,[4] W.-D. Möller,[4] A. Mosnier,[1] H. Padamsee,[3] C. Pagani,[7] M. Pekeler,[4,‡] H.-B. Peters,[4] O. Peters,[4] D. Proch,[4] K. Rehlich,[4] D. Reschke,[4] H. Safa,[1] T. Schilcher,[4,§] P. Schmüser,[8] J. Sekutowicz,[4] S. Simrock,[4] W. Singer,[4] M. Tigner,[3] D. Trines,[4] K. Twarowski,[4,10] G. Weichert,[4] J. Weisend,[4,‖] J. Wojtkiewicz,[4] S. Wolff,[4] and K. Zapfe[4]

[1]*CEA Saclay, Gif-sur-Yvette, France*
[2]*CERN, Geneve, Switzerland*
[3]*Cornell University, Ithaca, New York*
[4]*Deutsches Elektronen-Synchrotron, Hamburg, Germany*
[5]*FNAL, Batavia, Illinois*
[6]*INFN Frascati, Frascati, Italy*
[7]*INFN Milano, Milano, Italy*
[8]*II. Institut für Experimentalphysik, Universität Hamburg, Hamburg, Germany*
[9]*I.P.N. Orsay, Orsay, France*
[10]*Institute of Physics, Polish Academy of Sciences, Warsaw, Poland*
(Received 19 April 2000; published 22 September 2000)

The conceptional design of the proposed linear electron-positron collider TESLA is based on 9-cell 1.3 GHz superconducting niobium cavities with an accelerating gradient of $E_{acc} \geq 25$ MV/m at a quality factor $Q_0 \geq 5 \times 10^9$. The design goal for the cavities of the TESLA Test Facility (TTF) linac was set to the more moderate value of $E_{acc} \geq 15$ MV/m. In a first series of 27 industrially produced TTF cavities the average gradient at $Q_0 = 5 \times 10^9$ was measured to be 20.1 $\pm$ 6.2 MV/m, excluding a few cavities suffering from serious fabrication or material defects. In the second production of 24 TTF cavities, additional quality control measures were introduced, in particular, an eddy-current scan to eliminate niobium sheets with foreign material inclusions and stringent prescriptions for carrying out the electron-beam welds. The average gradient of these cavities at $Q_0 = 5 \times 10^9$ amounts to 25.0 $\pm$ 3.2 MV/m with the exception of one cavity suffering from a weld defect. Hence only a moderate improvement in production and preparation techniques will be needed to meet the ambitious TESLA goal with an adequate safety margin. In this paper we present a detailed description of the design, fabrication, and preparation of the TESLA Test Facility cavities and their associated components and report on cavity performance in test cryostats and with electron beam in the TTF linac. The ongoing research and development towards higher gradients is briefly addressed.

PACS numbers: 84.40.–x, 41.20.–q, 41.75.Ht, 74.60.–w

I. INTRODUCTION

In the past 30 years, electron-positron collisions have played a central role in the discovery and detailed investigation of new elementary particles and their interactions. The highly successful standard model of the unified electromagnetic and weak interactions and quantum chromodynamics, the quantum field theory of quark-gluon interactions, are to a large extent based on the precise data collected at electron-positron colliders. Important questions still remain to be answered, in particular, the origin of the masses of field quanta and particles—within the standard model explained in terms of the so-called Higgs mechanism—and the existence or nonexistence of supersymmetric particles which appear to be a necessary ingredient of any quantum field theory attempting to unify all four forces known in nature: the gravitational, weak, electromagnetic, and strong forces. There is general agreement in the high energy physics community that, in addition to the Large Hadron Collider under construction at CERN, a lepton collider will be needed to address these fundamental issues.

Electron-positron interactions in the center-of-mass (cm) energy range from 200 GeV to more than a TeV can no longer be realized in a circular machine such as LEP since the E^4 dependence of the synchrotron radiation loss would lead to prohibitive operating costs. Instead,

---

*Current address: CEA/IPSN, Fontenay, France.
†Current address: Center for Advanced Biotechnology, Boston University, Boston, Massachusetts.
‡Current address: ACCEL Instruments GmbH, Bergisch-Gladbach, Germany.
§Current address: Paul Scherrer Institut, Villigen, Switzerland.
‖Current address: SLAC, Stanford, California.

the linear collider concept must be employed. This new principle was successfully demonstrated with the Stanford Linear Collider (SLC) providing a cm energy of more than 90 GeV. Worldwide there are different design options towards the next generation of linear colliders in the 100 GeV to TeV regime. Two main routes are followed: colliders equipped with normal-conducting (nc) cavities (NLC, JLC, VLEPP, and CLIC) or with superconducting (sc) cavities (TESLA). The normal-conducting designs are based on high frequency structures (6 to 30 GHz), while the superconducting TESLA collider employs the comparatively low frequency of 1.3 GHz. The high conversion efficiency from primary electric power to beam power (about 20%) in combination with the small beam emittance growth in low-frequency accelerating structures makes the superconducting option an ideal choice for a high-luminosity collider.

The first international TESLA workshop was held in 1990 [1]. At that time superconducting rf cavities in particle accelerators were usually operated in the 5 MV/m regime. Such low gradients, together with the high cost of cryogenic equipment, would have made a superconducting linear electron-positron collider totally noncompetitive with the normal-conducting colliders proposed in the U.S. and Japan. The TESLA Collaboration, formally established in 1994 with the aim of developing a 500 GeV center-of-mass energy superconducting linear collider, set out with the ambitious goal of increasing the cost effectiveness of the superconducting option by more than 1 order of magnitude: first, by raising the accelerating gradient by a factor of 5 from 5 to 25 MV/m, and, second, by reducing the cost per unit length of the linac by using economical cavity production methods and a greatly simplified cryostat design. Important progress has been achieved in both directions; in particular, the gradient of 25 MV/m is essentially in hand, as will be shown below. To allow for a gradual improvement in the course of the cavity research and development (R&D) program, a more moderate goal of 15 MV/m was set for the TESLA Test Facility (TTF) linac [2].

The TESLA cavities are quite similar in their layout to the 5-cell 1.5 GHz cavities of the electron accelerator CEBAF in Newport News, Virginia, which were made by an industrial company [3]. These cavities exceeded the specified gradient of 5 MV/m considerably and, hence, offered the potential for further improvement. While the CEBAF cavity fabrication methods were adopted for TTF without major modifications, important new steps were introduced in the cavity preparation: (i) chemical removal of a thicker surface layer, (ii) a 1400 °C annealing with titanium getter to improve the Nb heat conductivity and to homogenize the material, (iii) rinsing with ultrapure water at high pressure (100 bar) to remove surface contaminants, and (iv) destruction of field emitters by a technique called high power processing.

The application of these techniques, combined with extremely careful handling of the cavities in a clean room environment, has led to a significant increase in accelerating field.

The TTF has been set up at DESY to provide the necessary infrastructure for the chemical and thermal treatment, clean room assembly, and testing of industrially produced multicell cavities. In addition, a 500 MeV electron linac is being built as a test bed for the performance of the sc accelerating structures with an electron beam of high bunch charge. At present, more than 30 institutes from Armenia, People's Republic of China, Finland, France, Germany, Italy, Poland, Russia, and the U.S. participate in the TESLA Collaboration and contribute to TTF.

The low frequency of 1.3 GHz permits the acceleration of long trains of particle bunches with very low emittance making a superconducting linac an ideal driver of a free electron laser (FEL) in the vacuum ultraviolet and x-ray regimes. For this reason, the TTF linac has recently been equipped with undulator magnets, and its energy will be upgraded to 1 GeV in the coming years to provide an FEL user facility in the nanometer wavelength range. An x-ray FEL facility with wavelengths below 1 Å is an integral part of the TESLA collider project [4].

The present paper is organized as follows: Sec. II is devoted to the basics of rf superconductivity and the properties and limitations of superconducting cavities for particle acceleration. The design of the TESLA cavities and the auxiliary equipment are presented in Sec. III. The fabrication and preparation steps of the cavities are described in Sec. IV. The test results obtained on all TTF cavities are presented in Sec. V, together with a discussion of errors and limitations encountered during cavity production at industry and the quality control measures taken. The rf control and cavity performance with electron beam in the TTF linac are described in Sec. VI. A summary and outlook are given in Sec. VII, where the ongoing research towards higher gradients is also briefly addressed.

II. BASICS OF RF SUPERCONDUCTIVITY AND PROPERTIES OF SUPERCONDUCTING CAVITIES FOR PARTICLE ACCELERATION

A. Basic principles of rf superconductivity and choice of superconductor

The existing large scale applications of superconductors in accelerators are twofold: in magnets and in accelerating cavities. While there are some common requirements, such as the demand for as high a critical temperature as possible,[1] there are also characteristic differences. In magnets operated with a dc or a low-frequency ac current, the

---

[1]The high-T_c ceramic superconductors have not yet found widespread application in magnets mainly due to technical difficulties in cable production and coil winding. Cavities with high-T_c sputter coatings on copper have shown much inferior performance in comparison to niobium cavities.

so-called "hard" superconductors are needed featuring high upper critical magnetic fields (15–20 T) and strong flux pinning in order to obtain high critical current density; such properties can only be achieved using alloys such as niobium-titanium or niobium-tin. In microwave applications the limitation of the superconductor is not given by the upper critical field but rather by the so-called "superheating field" which is well below 1 T for all known superconductors. Moreover, strong flux pinning appears undesirable in microwave cavities as it is coupled with hysteretic losses. Hence a "soft" superconductor must be used and pure niobium is still the best candidate although its critical temperature is only 9.2 K and the superheating field about 240 mT. Niobium-tin (Nb_3Sn) looks more favorable at first sight since it has a higher critical temperature of 18 K and a superheating field of 400 mT; however, the gradients achieved in Nb_3Sn coated single-cell copper cavities were below 15 MV/m, probably due to grain boundary effects in the Nb_3Sn layer [5]. For these reasons the TESLA Collaboration decided to use niobium as the superconducting material, as in all other large scale installations of sc cavities. Here two alternatives exist: the cavities are fabricated from solid niobium sheets or a thin niobium layer is sputtered onto the inner surface of a copper cavity. Both approaches have been successfully applied, the former at Cornell (CESR), KEK (TRISTAN), DESY (PETRA, HERA), Darmstadt (SDALINAC), Jefferson Lab (CEBAF), and other laboratories, the latter, in particular, at CERN in the electron-positron storage ring LEP. From the test results on existing cavities, the solid-niobium approach promised higher accelerating gradients, hence it was adopted as the baseline for the TTF cavity R&D program.

1. Surface resistance

In contrast to the dc case, superconductors are not free from energy dissipation in microwave fields. The reason is that the rf magnetic field penetrates a thin surface layer and induces oscillations of the electrons which are not bound in Cooper pairs. The number of these "free electrons" drops exponentially with temperature. According to the Bardeen-Cooper-Schrieffer (BCS) theory of superconductivity the surface resistance in the range $T < T_c/2$ is given by the expression

$$R_{BCS} \propto \frac{\omega^2}{T} \exp(-1.76\, T_c/T), \qquad (2.1)$$

where $f = \omega/2\pi$ is the microwave frequency. In the two-fluid model of superconductors one can derive a refined expression for the surface resistance [6,7]

$$R_{BCS} = \frac{1}{2}\, \omega^2 \mu_0^2 \Lambda^3 \sigma_n. \qquad (2.2)$$

Here σ_n is the normal-state conductivity of the material, and Λ is an effective penetration depth, given by
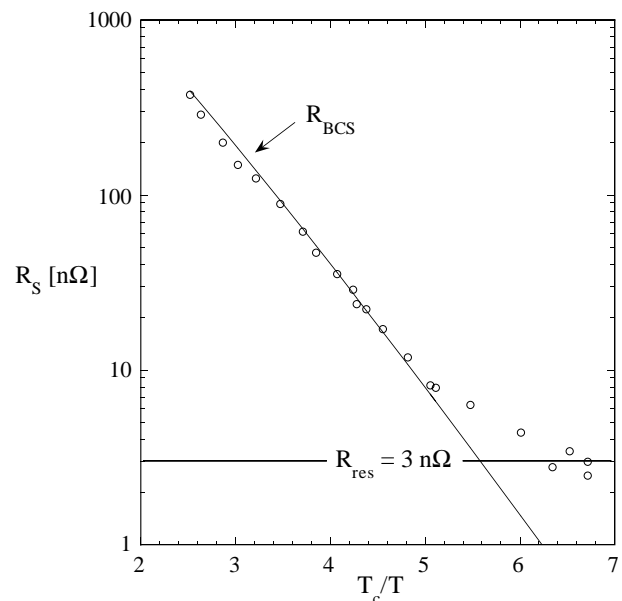

FIG. 1. The surface resistance of a 9-cell TESLA cavity plotted as a function of T_c/T. The residual resistance of 3 nΩ corresponds to a quality factor of $Q_0 = 10^{11}$.

$$\Lambda = \lambda_L \sqrt{1 + \xi_0/\ell}\,,$$

where λ_L is the London penetration depth, ξ_0 is the coherence length, and ℓ is the mean free path of the unpaired electrons. The fact that σ_n is proportional to the mean free path ℓ leads to the surprising conclusion that the surface resistance does not assume its minimum value when the superconductor is as pure as possible ($\ell \gg \xi_0$) but rather in the range $\ell \approx \xi_0$. For niobium, the BCS surface resistance at 1.3 GHz amounts to about 800 nΩ at 4.2 K and drops to 15 nΩ at 2 K; see Fig. 1. The exponential temperature dependence is the reason that operation at 1.8–2 K is essential for achieving high accelerating gradients in combination with very high quality factors. Superfluid helium is an excellent coolant owing to its high heat conductivity.

In addition to the BCS term there is a residual resistance R_{res} caused by impurities, frozen-in magnetic flux, or lattice distortions. This term is temperature independent and amounts to a few nΩ for very pure niobium but may readily increase if the surface is contaminated.

2. Heat conduction in niobium

The heat produced at the inner cavity surface has to be guided through the cavity wall to the superfluid helium bath. Two quantities characterize the heat flow: the thermal conductivity of the bulk niobium and the temperature drop at the niobium-helium interface caused by the Kapitza resistance. For niobium with a residual resistivity

ratio[2] RRR of $\mathcal{R}_{\mathrm{RRR}} = 500$, the two contributions to the temperature rise at the inner cavity surface are about equal. The thermal conductivity of niobium at cryogenic temperatures scales approximately with the RRR, a rule of thumb being

$$\lambda(4.2 \text{ K}) \approx 0.25 \mathcal{R}_{\mathrm{RRR}} \text{ [W/mK]}.$$

However, λ is strongly temperature dependent and drops by about 1 order of magnitude when lowering the temperature to 2 K, as shown in Fig. 2.

Impurities influence the RRR and the thermal conductivity of niobium. Bulk niobium is contaminated by interstitial (mostly hydrogen, carbon, nitrogen, oxygen) and metallic impurities (mostly tantalum). The resulting RRR can be calculated by summing the individual contributions [10]

$$\mathcal{R}_{\mathrm{RRR}} = \left(\sum_i f_i/r_i \right)^{-1}, \qquad (2.3)$$

where the f_i denotes the fractional contents of impurity i (measured in wt. ppm) and the r_i denotes the corresponding resistivity coefficients which are listed in Table I.

A good thermal conductivity is the main motivation for using high purity niobium with RRR ≈ 300 as the material for cavity production. The RRR may be further improved by postpurification of the entire cavity (see Sec. V).

The Kapitza conductance depends on temperature and surface conditions. For pure niobium in contact
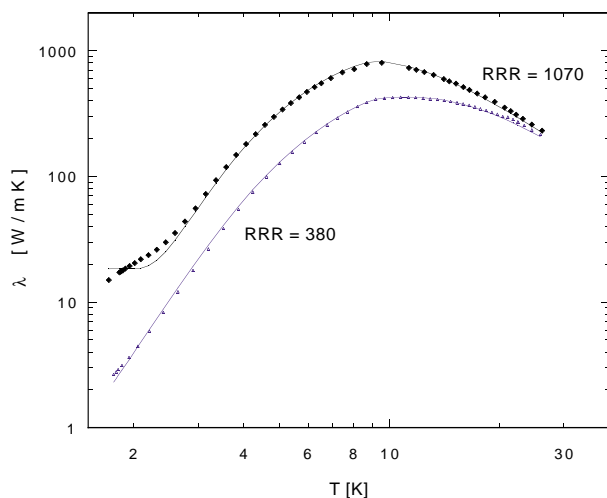

FIG. 2. The measured heat conductivity in niobium as a function of temperature [8]. Continuous curves: parametrization by Bonin, using the RRR and the average grain size as input parameters [9]. These data do not show an enhancement at 2 K (the so-called "phonon peak") which was observed in some earlier experiments [5].

TABLE I. Resistivity coefficients of common impurities in Nb [10].

Impurity atom i	N	O	C	H	Ta
r_i in 10^4 wt. ppm	0.44	0.58	0.47	0.36	111

with superfluid helium at 2 K it amounts to about 6000 W/(m²K) [11].

3. Influence of magnetic fields

Superheating field. Superconductivity breaks down when the rf magnetic field exceeds the critical field of the superconductor. In the high frequency case the so-called superheating field is relevant which, for niobium, is about 20% higher than the thermodynamical critical field of 200 mT [12,13].

Trapped magnetic flux. Niobium is, in principle, a soft type II superconductor without flux pinning. In practice, however, weak magnetic dc fields are not expelled upon cooldown but remain trapped in the niobium. Each flux line contains a normal-conducting core whose area is roughly $\pi \xi_0^2$. The coherence length ξ_0 amounts to 40 nm in Nb. Trapped magnetic dc flux therefore results in a surface resistance [6]

$$R_{\mathrm{mag}} = (B_{\mathrm{ext}}/2B_{c2})R_n, \qquad (2.4)$$

where B_{ext} is the externally applied field, B_{c2} is the upper critical field, and R_n is the surface resistance in the normal state.[3] At 1.3 GHz the surface resistance caused by trapped flux amounts to 3.5 nΩ/μT for niobium. Cavities which are not shielded from the Earth's magnetic field are therefore limited to Q_0 values below 10^9.

B. Advantages and limitations of superconducting cavities

The fundamental advantage of superconducting cavities is the extremely low surface resistance of about 10 nΩ at 2 K. The typical quality factors of normal conducting cavities are 10^4–10^5 while for sc cavities they may exceed 10^{10}, thereby reducing the rf losses by 5 to 6 orders of magnitude. In spite of the low efficiency of refrigeration there are considerable savings in primary electric power. Only a tiny fraction of the incident rf power is dissipated in the cavity walls, most of it is either transferred to the beam or reflected into a load.

The physical limitation of a sc resonator is given by the requirement that the rf magnetic field at the inner surface has to stay below the superheating field of the superconductor (200–240 mT for niobium). For the TESLA cavities this implies a maximum accelerating field of 50–60 MV/m. In principle, the quality factor should

---

[2]RRR is defined as the ratio of the resistivities at room temperature and at liquid helium temperature. The low temperature resistivity is measured either just above T_c or at 4.2 K, applying a magnetic field to assure the normal state.

[3]Benvenuti *et al.* [14] attribute the magnetic surface resistance in niobium sputter layers to flux flow.

stay roughly constant when approaching this fundamental superconductor limit, but in practice the "excitation curve" $Q_0 = Q_0(E_{acc})$ ends at considerably lower values, often accompanied with a strong decrease of Q_0 towards the highest gradient reached in the cavity. The main reasons for the performance degradation are excessive heating at impurities on the inner surface, field emission of electrons, and multipacting.[4]

Thermal instability and field emission

One basic limitation of the maximum field in a superconducting cavity is thermal instability. Temperature mapping at the outer cavity wall usually reveals that the heating by rf losses is not uniform over the whole surface but that certain spots exhibit larger temperature rises, often beyond the critical temperature of the superconductor. Hence the cavity becomes partially normal conducting, associated with strongly enhanced power dissipation. Because of the exponential increase of surface resistance with temperature, this may result in a runaway effect and eventually a quench of the entire cavity. Analytical models as well as numerical simulations are available to describe such an avalanche effect. Input parameters are the thermal conductivity of the superconductor, the size and resistance of the normal conducting spot, and the Kapitza resistance. The tolerable defect size depends on the RRR of the material and the desired field level. As a typical number, the diameter of a normal-conducting spot must exceed 50 μm to be able to initiate a thermal instability at 25 MV/m for RRR > 200.

There have been many attempts to identify defects which were localized by temperature mapping. Examples of defects are drying spots, fibers from tissues, foreign material inclusions, weld splatter, and cracks in the welds. There are two obvious and successful methods for reducing the danger of thermal instability: (i) avoid defects by preparing and cleaning the cavity surface with extreme care

---

[4]"Multipacting" is a commonly used abbreviation for "multiple impacting" and designates the resonant multiplication of field emitted electrons which gain energy in the rf electromagnetic field and impact on the cavity surface where they induce secondary electron emission.

and (ii) increase the thermal conductivity of the superconductor. Considerable progress has been achieved in both aspects over the past ten years.

Field emission of electrons from sharp tips is the most severe limitation in high-gradient superconducting cavities. In field-emission loaded cavities, the quality factor drops exponentially above a certain threshold and x rays are observed. The field emission current density is given by the Fowler-Nordheim equation [15]

$$j_{FE} = c_1 E_{loc}^{2.5} \exp\left(-\frac{c_2}{\beta E_{loc}}\right), \qquad (2.5)$$

where E_{loc} is the local electric field, β is a so-called field enhancement factor, and c_1 and c_2 are constants. There is experimental evidence that small particles on the cavity surface (e.g., dust) act as field emitters. Therefore, perfect cleaning, for example by high-pressure water rinsing, is the most effective remedy against field emission. By applying this technique it has been possible to raise the threshold for field emission in multicell cavities from about 10 MV/m to more than 20 MV/m in the past few years.

The topics of thermal instability and field emission are discussed at much greater detail in the book by Padamsee, Knobloch, and Hays [16].

III. DESIGN OF THE TESLA CAVITIES

A. Overview

The TTF cavity is a 9-cell standing wave structure of about 1 m length whose lowest TM mode resonates at 1300 MHz. A photograph is shown in Fig. 3. The cavity is made from solid niobium and is cooled by superfluid helium at 2 K.

Each 9-cell cavity is equipped with its own titanium helium tank, a tuning system driven by a stepping motor, a coaxial rf power coupler capable of transmitting more than 200 kW, a pickup probe, and two higher-order mode (HOM) couplers. To reduce the cost for cryogenic installations, eight cavities and a superconducting quadrupole are mounted in a common vacuum vessel and constitute the so-called cryomodule of the TTF linac, shown in Fig. 4. Within the module the cavity beam pipes are joined by stainless steel bellows and flanges with metallic gaskets. The cavities are attached to a rigid 300 mm diameter helium supply tube which provides positional accuracy of the cavity axes of better than 0.5 mm. Invar rods ensure
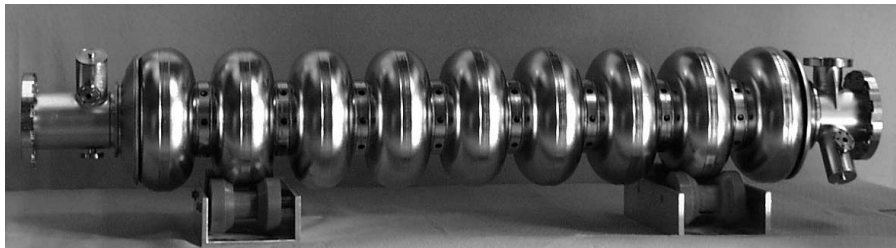

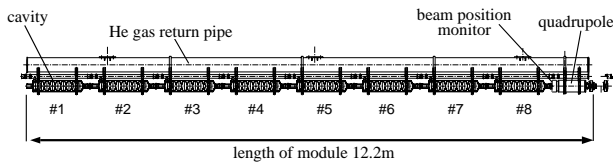FIG. 3.   Superconducting 1.3 GHz 9-cell cavity for the TESLA Test Facility.

FIG. 4. Cryogenic module of the TESLA Test Facility linac comprising eight 9-cell cavities and a superconducting quadrupole.

that the distance between adjacent cavities remains constant during cooldown. Radiation shields at 5 and 60 K together with 30 layers of superinsulation limit the static heat load on the 2 K level to less than 3 W for the 12 m long module.

B. Layout of the TESLA cavities

1. Choice of frequency

The losses in a microwave cavity are proportional to the product of conductor area and surface resistance. For a given length of a multicell resonator, the area scales with $1/f$ while the surface resistance of a superconducting cavity scales with f^2 for $R_{\mathrm{BCS}} \gg R_{\mathrm{res}}$ and is independent of f for $R_{\mathrm{BCS}} \ll R_{\mathrm{res}}$. At an operating temperature $T = 2$ K, the BCS term dominates above 3 GHz and, hence, the losses grow linearly with frequency, whereas, for frequencies below 300 MHz, the residual resistance dominates and the losses grow with $1/f$. To minimize the dissipation in the cavity wall one should therefore select f in the range 300 MHz to 3 GHz.

Cavities in the 350 to 500 MHz regime are in use in electron-positron storage rings. Their large size is advantageous to suppress wake field effects and higher-order mode losses. However, for a linac of several 10 km length the niobium and cryostat costs for these bulky cavities would be prohibitive, hence a higher frequency has to be chosen. Considering material costs $f = 3$ GHz might appear the optimum, but there are compelling arguments for choosing about half this frequency:

(i) The wake field losses scale with the second to third power of the frequency ($W_{\parallel} \propto f^2, W_{\perp} \propto f^3$). Beam emittance growth and beam-induced cryogenic losses are therefore much higher at 3 GHz.

(ii) The f^2 dependence of the BCS resistance sets an upper limit[5] of about 30 MV/m at 3 GHz, hence, choosing this frequency would definitely preclude a possible upgrade of TESLA to 35–40 MV/m [17].

The choice for 1.3 GHz was motivated by the availability of high power klystrons.

---

[5]See Fig. 11.22 in [16].

2. Cavity geometry

A multicell resonator is advantageous for maximizing the active acceleration length in a linac of a given size. With the increasing number of cells per cavity, however, difficulties arise from trapped modes, uneven field distribution in the cells, and too high power requirements on the input coupler. Extrapolating from the experience with 4-cell and 5-cell cavities, a 9-cell structure appeared manageable. A side view of the TTF cavity with the beam tube sections and the coupler ports is given in Fig. 5.

The design of the cell shape was guided by the following considerations: (i) a spherical contour near the equator with low sensitivity for multipacting, (ii) minimization of electric and magnetic fields at the cavity wall to reduce the danger of field emission and thermal breakdown, and (iii) a large iris radius to reduce wake field effects.

The shape of the cell was optimized using the code URMEL [18]. The resonator is operated in the π mode with 180° phase difference between adjacent cells. The longitudinal dimensions are determined by the condition that the electric field has to be inverted in the time a relativistic particle needs to travel from one cell to the next. The separation between two irises is therefore $c/(2f)$. The iris radius R_{iris} influences the cell-to-cell coupling[6] k_{cell}, the excitation of higher-order modes, and other important cavity parameters, such as the ratio of the peak electric (magnetic) field at the cavity wall to the accelerating field and the ratio (R/Q) of shunt impedance to the quality factor. For the TESLA Test Facility cavities, $R_{\mathrm{iris}} = 35$ mm was chosen, leading to $k_{\mathrm{cell}} = 1.87\%$ and $E_{\mathrm{peak}}/E_{\mathrm{acc}} = 2$. The most important parameters are listed in Table II.

The contour of a half-cell is shown in Fig. 6. It is composed of a circular arc around the equator region and an elliptical section near the iris. The dimensions are listed in Table III. The half-cells at the end of the 9-cell resonator need a slightly different shape to ensure equal field amplitudes in all 9 cells. In addition, there is a slight asymmetry
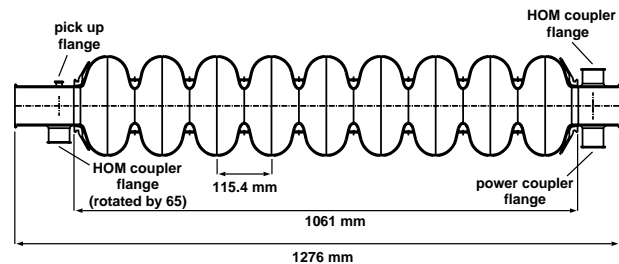

FIG. 5. Side view of the 9-cell TTF cavity with the ports for the main power coupler and two HOM couplers.

---

[6]The coupling coefficient is related to the frequencies of the coupled modes in the 9-cell resonator by the formula $f_n = f_0/\sqrt{1 + 2\,k_{\mathrm{cell}}\cos(n\pi/9)}$ where f_0 is the resonant frequency of a single cell and $1 \leq n \leq 9$.

TABLE II.   TTF cavity design parameters.[a]

Type of accelerating structure	Standing wave
Accelerating mode	TM_{010}, π mode
Fundamental frequency	1300 MHz
Design gradient E_{acc}	25 MV/m
Quality factor Q_0	$>5 \times 10^9$
Active length L	1.038 m
Number of cells	9
Cell-to-cell coupling	1.87%
Iris diameter	70 mm
Geometry factor	270 Ω
R/Q	518 Ω
E_{peak}/E_{acc}	2.0
B_{peak}/E_{acc}	4.26 mT MV^{-1} m^{-1}
Tuning range	±300 kHz
$\Delta f/\Delta L$	315 kHz/mm
Lorentz force detuning at 25 MV/m	≈600 Hz
Q_{ext} of input coupler	3×10^6
Cavity bandwidth at $Q_{ext} = 3 \times 10^6$	430 Hz
rf pulse duration	1330 μs
Repetition rate	5 Hz
Fill time	530 μs
Beam acceleration time	800 μs
rf power peak/average	208 kW/1.4 kW
Number of HOM couplers	2
Cavity longitudinal loss factor $k_\parallel$ for $\sigma_z = 0.7$ mm	10.2 V/pC
Cavity transversal loss factor $k_\perp$ for $\sigma_z = 0.7$ mm	15.1 V pC^{-1} m^{-1}
Parasitic modes with the highest impedance: type	TM_{011}
$\pi/9$ (R/Q)/frequency	80 Ω/2454 MHz
$2\pi/9$ (R/Q)/frequency	67 Ω/2443 MHz
Bellows longitudinal loss factor $k_\parallel$ for $\sigma_z = 0.7$ mm	1.54 V/pC
Bellows transversal loss factor $k_\perp$ for $\sigma_z = 0.7$ mm	1.97 V pC^{-1} m^{-1}

[a]Following common usage in ac circuits and the convention adopted in Ref. [19], p. 523, we define the shunt impedance by the relation $R = V^2/2P$, where P is the dissipated power and V is the peak voltage in the equivalent parallel LCR circuit. Note that another definition is common, which has also been used in the TESLA Conceptual Design Report, $R = V^2/P$, leading to a factor of 2 larger shunt impedance.

between the left and right end cell which prevents trapping of higher-order modes (see Sec. III E).

3. Lorentz-force detuning and cavity stiffening

The electromagnetic field exerts a Lorentz force on the currents induced in a thin surface layer. The resulting pressure acting on the cavity wall

$$p = \frac{1}{4}(\mu_0 H^2 - \varepsilon_0 E^2) \qquad (3.1)$$

leads to a deformation of the cells in the μm range and a change ΔV of their volume. The consequence is a frequency shift according to Slater's rule
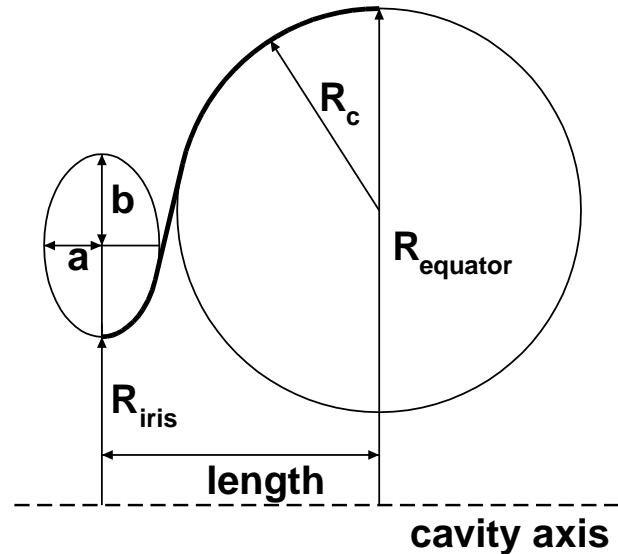

FIG. 6.   Contour of a half-cell.

$$\frac{\Delta f}{f_0} = \frac{1}{4W} \int_{\Delta V} (\varepsilon_0 E^2 - \mu_0 H^2)\, dV. \qquad (3.2)$$

Here,

$$W = \frac{1}{4} \int_V (\varepsilon_0 E^2 + \mu_0 H^2)\, dV \qquad (3.3)$$

is the stored energy and f_0 is the resonant frequency of the unperturbed cavity. The computed frequency shift at 25 MV/m amounts to 900 Hz for an unstiffened cavity of 2.5 mm wall thickness. The bandwidth of the cavity equipped with the main power coupler ($Q_{ext} = 3 \times 10^6$) is about 430 Hz, hence, a reinforcement of the cavity is needed. Niobium stiffening rings are welded in between adjacent cells as shown in Fig. 7. They reduce the frequency shift to about 500 Hz for a 1.3 ms long rf pulse[7]; see Fig. 26.

The deformation of the stiffened cell is negligible near the iris where the electric field is large, but remains nearly the same as in the unstiffened cell near the equator where the magnetic field dominates. The deformation in this region can be reduced only by increasing the wall thickness.

TABLE III.   Half-cell shape parameters (all dimensions in mm).

Cavity shape parameter	Midcup	Endcup 1	Endcup 2
Equator radius R_{equat}	103.3	103.3	103.3
Iris radius R_{iris}	35	39	39
Radius R_{arc} of circular arc	42.0	40.3	42
Horizontal half axis a	12	10	9
Vertical half axis b	19	13.5	12.8
Length l	57.7	56.0	57.0

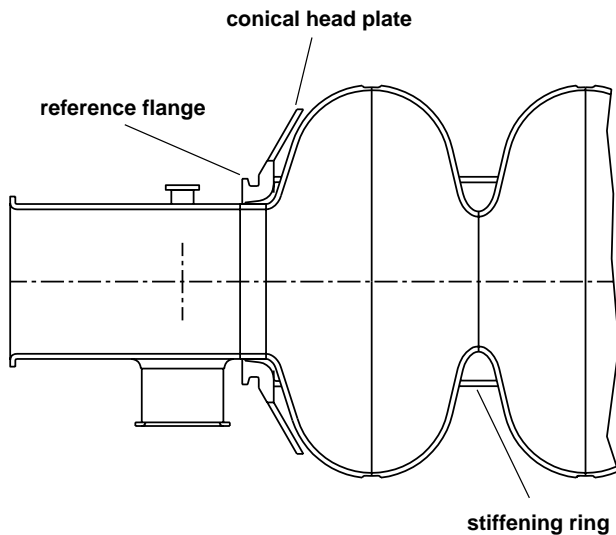[7]Part of this shift is due to an elastic deformation of the tuning mechanism.

FIG. 7.   The end section of a cavity with stiffening ring, conical head plate for welding into the helium tank, and reference flange for alignment.

4. Magnetic shielding

As shown in Sec. II A 3, the ambient magnetic field must be shielded to a level of about a μT to reduce the magnetic surface resistance to a few nΩ. This is accomplished with a two-stage passive shielding, provided by the conventional steel vacuum vessel of the cryomodule and a high-permeability cylinder around each cavity. To remove the remanence from the steel vessel, the usual demagnetization technique is applied. The resulting attenuation of the ambient field is found to be better than expected from a cylinder without any remanence. The explanation is that the procedure does not really demagnetize the steel but rather *remagnetizes* it in such a way that the axial component of the ambient field is counteracted. This interpretation (see also Ref. [20]) becomes obvious if the cylinder is turned by 180°: in that case the axial field measured inside the steel cylinder is almost twice as large as the ambient longitudinal field component; see Fig. 8(a).

The shielding cylinders of the cavities are made from Cryoperm[8] which retains a high permeability of more than 10 000 when cooled to liquid helium temperature. Figure 8(b) shows the measured horizontal, vertical, and axial components inside a cryoperm shield at room temperature, which was exposed to the Earth's field. The combined action of remagnetized vacuum vessel and cryoperm shield is more than adequate to reduce the ambient field to the level of some μT. An exception is the end cells of the first and the last cavity near the end of the cryomodule where the vessel is not effective in attenuating longitudinal fields. Here an active field compensation by means of Helmholtz

---

[8]Cryoperm is made by Vacuumschmelze Hanau, Germany.
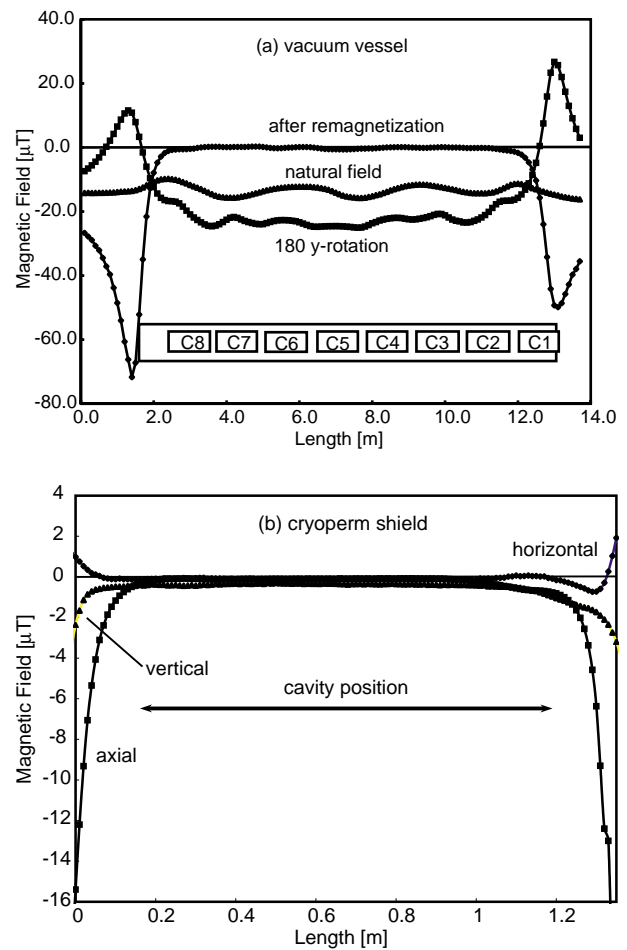
FIG. 8.   Shielding of the Earth's magnetic field. (a) Shielding of an axial component by the steel vacuum vessel of the cryomodule. Also shown is the arrangement of the cavity string in the vessel. (b) Shielding of the axial, horizontal, and vertical field components by the cryoperm cylinder surrounding the cavity (measured without vacuum vessel).

coils could reduce the fringe field at the last cavity to a harmless level.

C. Helium vessel and tuning system

The helium tank contains the superfluid helium needed for cooling and serves at the same time as a mechanical support of the cavity and as a part of the tuning mechanism. The tank is made from titanium whose differential thermal contraction relative to niobium is 20 times smaller than for stainless steel. Cooldown produces a stress of only 3 MPa in a cavity that was stress free at room temperature. Titanium has the additional advantage that it can be directly electron-beam (EB) welded to niobium while stainless steel-niobium joints would require an intermediate metal layer.

The assembly of the cavity and helium tank proceeds in the following sequence: a titanium bellows is electron-beam welded to the conical Nb head plate at one side of the cavity, a titanium ring is EB welded to the conical Nb

head plate at the other side (see Fig. 7). The cavity is then inserted into the tank and the bellows as well as the titanium ring are tungsten inert gas (TIG) welded to the Ti vessel.

The tuning system consists of a stepping motor with a gear box and a double lever arm. The moving parts operate at 2 K in vacuum. The tuning range is about ± 1 mm, corresponding to a frequency range of ± 300 kHz. The resolution is 1 Hz. The tuning system is adjusted in such a way that after cooldown the cavity is always under compressive force to avoid a backlash if the force changes from pushing to pulling.

D. Main power coupler

1. Design requirements

A critical component of a superconducting cavity is the power input coupler. Several coaxial couplers have been developed for TTF [21], consisting of a "cold part," which is mounted on the cavity in the clean room and closed by a ceramic window, and a "warm part," which is assembled after installation of the cavity in the cryomodule. The warm section contains the transition from waveguide to coaxial line. This part is evacuated and sealed against the air-filled waveguide by a second ceramic window. The elaborate two-window solution was chosen to get optimum protection of the cavity against contamination during mounting in the cryomodule and against window fracture during linac operation.

The couplers must allow for some longitudinal motion[9] inside the 12 m long cryomodule when the cavities are cooled down from room temperature to 2 K. For this reason, bellows in the inner and outer conductors of the coaxial line are needed. Since the coupler connects the room-temperature waveguide with the 2 K cavity, a compromise must be found between a low thermal conductivity and a high electrical conductivity. This is achieved by several thermal intercepts and by using stainless steel pipes or bellows with a thin copper plating ($10-20$ μm) at the radio frequency surface. The design heat loads of 6 W at 70 K, 0.5 W at 4 K, and 0.06 W at 2 K have been undercut in practice.

2. Electrical properties

An instantaneous power of 210 kW has to be transmitted to provide a gradient of 25 MV/m for an 800 μs long beam pulse of 8 mA. The filling time of the cavity amounts to 530 μs and the decay time, after the beam pulse is over, to an additional 500 μs. At the beginning of the filling,

most of the rf wave is reflected leading to voltage enhancements by a factor of 2. The external quality factor of the coupler is $Q_{ext} = 3 \times 10^6$ at 25 MV/m. By moving the inner conductor of the coaxial line, Q_{ext} can be varied in the range $1 \times 10^6 - 9 \times 10^6$ to allow not only for different beam loading conditions but also to facilitate an *in situ* high power processing of the cavities. This feature has proved extremely useful on several occasions to eliminate field emitters that entered the cavities at the last assembly stage.

3. Input coupler A

The coupler version A is shown in Fig. 9. It has a conical ceramic window at 70 K and a commercial planar waveguide window at room temperature.

A conical shape was chosen for the cold ceramic window to obtain broad band impedance matching. The Hewlett-Packard high frequency structure simulator program HFSS was used to model the window and to optimize the shape of the tapered inner conductor. The reflected power is below 1%. The ceramic window is made from Al_2O_3 with a purity of 99.5%. Oxygen-free high-conductance copper rings are brazed to the ceramic using Au/Cu (35%/65%) braze alloy. The inner conductors on each side of the ceramic are electron-beam welded, the outer conductors are TIG welded. The ceramic is coated on both sides with a 10 nm titanium nitride layer to reduce multipacting.

The waveguide-to-coaxial transition is realized using a cylindrical knob such as the impedance-transforming device and a planar waveguide window. Matching posts are required on the air side of the window for impedance matching at 1.3 GHz.

4. Input couplers B, C

Coupler version B also uses a planar waveguide window and a doorknob transition from the waveguide to the coaxial line, but a cylindrical ceramic window at 70 K without direct view of the beam. Because of a shortage in commercial waveguide windows, a third type, C, was developed using a cylindrical window also at the waveguide-
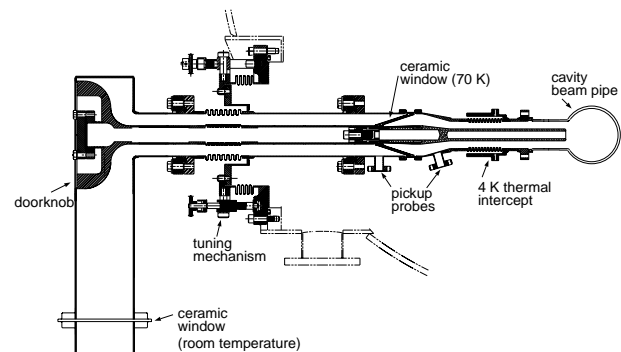

FIG. 9. A simplified view of the power input coupler version A.

---

[9]The motion of the coupler ports is up to 15 mm in the first cryomodules but has been reduced to about 1 mm in the most recent cryostat design by fixing the distance between neighboring cavities with invar rods.

coaxial transition. It features a 60 mm diameter coaxial line with reduced sensitivity to multipacting and the possibility of applying a dc potential to the center conductor. In the case of the LEP couplers [22], a dc bias has proved very beneficial in suppressing multipacting. Similar observations were made at DESY. All couplers needed some conditioning but have then performed according to specification.

E. Higher-order modes

The intense electron bunches excite eigenmodes of higher frequency in the resonator which must be damped to avoid multibunch instabilities and beam breakup. This is accomplished by extracting the stored energy via HOM couplers mounted on the beam pipe sections of the 9-cell resonator. A problem arises from "trapped modes" which are concentrated in the center cells and have a low field amplitude in the end cells. An example is the TE_{121} mode. By an asymmetric shaping of the end half-cells, one can enhance the field amplitude of the TE_{121} mode in one end cell while preserving the "field flatness" of the fundamental mode and also the good coupling of the HOM couplers to the untrapped modes TE_{111}, TM_{110}, and TM_{011}. The effects of asymmetric end cell tuning are sketched in Fig. 10.

The two polarization states of dipole modes would, in principle, require two orthogonal HOM couplers at each side of the cavity. In a string of cavities, however, this complexity can be avoided since the task of the "orthogonal" HOM coupler can be taken over by the HOM coupler of the neighboring cavity. The viability of this idea was verified in measurements.

HOM coupler design

The HOM couplers are mounted at both ends of the cavity with a nearly perpendicular orientation[10] to ensure
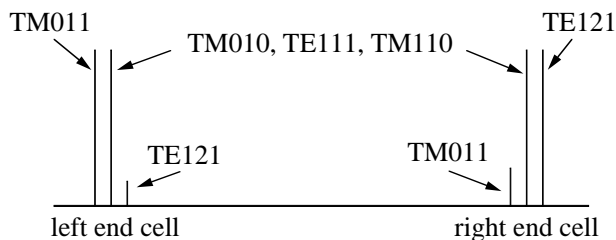

FIG. 10. The effect of asymmetric end cell shaping on various modes. The main accelerating mode TM_{010} and the higher modes TE_{111} and TM_{110} are not affected while TM_{011} is enhanced in the left end cell and TE_{121} is enhanced in the right end cell. Using HOM couplers at both ends, all higher-order modes can be extracted.

---

[10]The angle between the two HOM couplers is not 90° but 115° to also provide damping of quadrupole modes.

damping of dipole modes of either polarization. A 1.3 GHz notch filter is incorporated to prevent energy extraction from the accelerating mode. Two types of HOM couplers have been developed and tested, one mounted on a flange, the other welded to the cavity.

The demountable HOM coupler is shown in Fig. 11(a). An antenna loop couples mainly to the magnetic field for TE modes and to the electric field for TM modes. The pickup antenna is capacitively coupled to an external load. The 1.3 GHz notch filter is formed by the inductance of the loop and the capacity at the 1.9 mm wide gap between loop and wall. A niobium bellows permits tuning of the filter without opening the cavity vacuum. The antenna is thermally connected to the 2 K helium bath. In a continuous wave (cw) test at an accelerating field of 21 MV/m the antenna reached a maximum temperature of 4 K, which is totally uncritical.

The welded version of the HOM coupler is shown in Fig. 11(b). It resembles the couplers used in the 500 MHz HERA cavities which have been operating for several years without quenches. The good cooling of the superconducting inner conductor by two stubs makes the design insensitive to γ radiation and electron bombardment.

Both HOM couplers permit tuning of the fundamental mode rejection filter when mounted on the cavity. It is possible to achieve a Q_{ext} of more than 10^{11} thereby limiting power extraction to less than 50 mW at 25 MV/m.
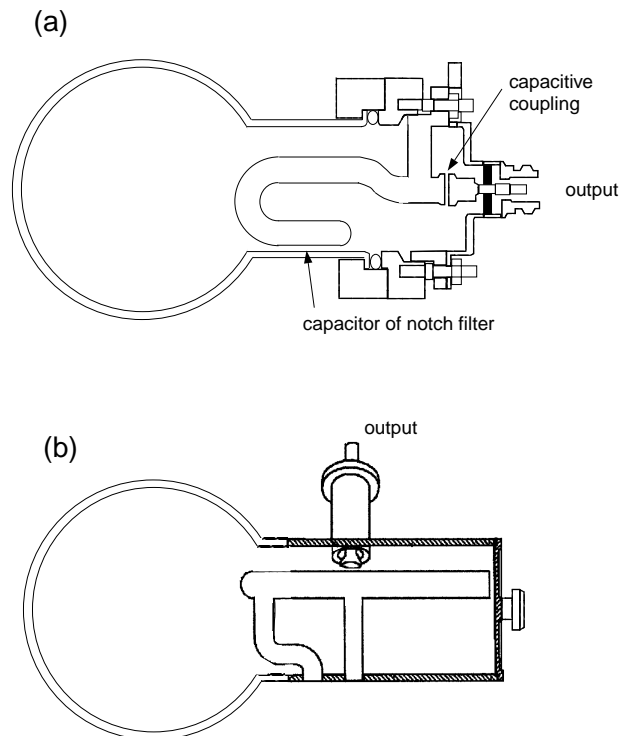

FIG. 11. The higher-order-mode couplers: (a) demountable HOM coupler and (b) welded HOM coupler.

IV. CAVITY FABRICATION AND PREPARATION

A. Cavity fabrication

1. Niobium properties

The 9-cell resonators are made from 2.8 mm thick sheet niobium by deep drawing of half-cells, followed by trimming and electron beam welding. Niobium of high purity is needed. Tantalum with a typical concentration of 500 ppm is the most important metallic impurity. Among the interstitially dissolved impurities, oxygen is dominant due to the high affinity of Nb for O_2 above 200 °C. Interstitial atoms act as scattering centers for the unpaired electrons and reduce the RRR and the thermal conductivity; see Sec. II A. The niobium ingot is highly purified by several remelting steps in a high vacuum electron beam furnace. This procedure reduces the interstitial oxygen, nitrogen, and carbon contamination to a few ppm. The niobium specification for the TTF cavities is listed in Table IV.

After forging and sheet rolling, the 2.8 mm thick Nb sheets are degreased, a 5 μm surface layer is removed by etching, and then the sheets are annealed for 1–2 h at 700 °C–800 °C in a vacuum oven at a pressure of 10^{-5}–10^{-6} mbar to achieve full recrystallization and a uniform grain size of about 50 μm.

2. Deep drawing and electron-beam welding

Half-cells are produced by deep drawing. The dies are usually made from a high yield strength aluminum alloy. To achieve the small curvature required at the iris, an additional step of forming, e.g., coining, may be needed. The half-cells are machined at the iris and the equator. At the iris the half-cell is cut to the specified length (allowing for weld shrinkage) while at the equator an extra length of 1 mm is left to retain the possibility of a precise length trimming of the dumbbell after frequency measurement (see below). The accuracy of the shape is controlled by sandwiching the half-cell between two metal plates and measuring the resonance frequency. The half-cells are thoroughly cleaned by ultrasonic degreasing, 20 μm chemical etching, and ultrapure water rinsing. Two half-cells are then joined at the iris with an EB weld to form a "dumbbell." The EB welding is usually done from the

TABLE IV. Technical specification for niobium used in TTF cavities

Impurity content in ppm (wt.)				Mechanical properties	
Ta	≤500	H	≤2	RRR	≥300
W	≤70	N	≤10	Grain size	≈50 μm
Ti	≤50	O	≤10	Yield strength	>50 MPa
Fe	≤30	C	≤10	Tensile strength	>100 MPa
Mo	≤50			Elongation at break	30%
Ni	≤30			Vickers hardness	
				HV 10	≤50

inside to ensure a smooth weld seam at the location of the highest electric field in the resonator. Since niobium is a strong getter material for oxygen, it is important to carry out the EB welds in a sufficiently good vacuum. Tests have shown that RRR = 300 niobium is not degraded by welding at a pressure of less than 5×10^{-5} mbar.

The next step is the welding of the stiffening ring. Here the weld shrinkage may lead to a slight distortion of the cell shape which needs to be corrected. Afterwards, frequency measurements are made on the dumbbells to determine the correct amount of trimming at the equators. After proper cleaning by a 30 μm etching, the dumbbells are visually inspected. Defects and foreign material imprints from previous fabrication steps are removed by grinding. After the inspection and proper cleaning (a few μm etching followed by ultraclean water rinsing and clean room drying), eight dumbbells and two beam-pipe sections with attached end half-cells are stacked in a precise fixture to carry out the equator welds which are done from the outside. The weld parameters are chosen to achieve full penetration. A reliable method for obtaining a smooth weld seam of a few mm width at the inner surface is to raster a slightly defocused beam in an elliptic pattern and to apply 50% of beam power during the first weld pass and 100% of beam power in the second pass.

B. Cavity treatment

Experience has shown that a damage layer of the order of 100 μm has to be removed from the inner cavity surface to obtain good rf performance in the superconducting state. The standard method applied at DESY and many other laboratories is called buffered chemical polishing (BCP), using an acid mixture of HF (48%), HNO_3 (65%), and H_3PO_4 (85%) in the ratio 1:1:2 (at CEBAF the ratio was 1:1:1). The preparation steps adopted at DESY for the industrially produced TTF cavities are as follows: A layer of 80 μm is removed by BCP from the inner surface and 30 μm from the outer surface.[11] The cavities are rinsed with ultraclean water and dried in a class 100 clean room. The next step is a 2 h annealing at 800 °C in an ultrahigh vacuum (UHV) oven which serves to remove dissolved hydrogen from the niobium and relieves mechanical stress in the material. In the initial phase of the TTF program many cavities were tested after this step, applying a 20 μm BCP and ultraclean water rinsing before mounting in the cryostat and cooldown.

Presently, the cavities are rinsed with clean water after the 800 °C treatment and then immediately transferred to another UHV oven in which they are heated to

---

[11]These numbers are determined by weighing the cavity before and after etching and represent, therefore, the average over the whole surface. Frequency measurements indicate that more material is etched away at the iris than at the equator.

1350 °C–1400 °C. At this temperature, all dissolved gases diffuse out of the material and the RRR increases by about a factor of 2 to values around 500. To capture the oxygen coming out of the niobium and to prevent oxidation by the residual gas in the oven (pressure $<10^{-7}$ mbar), a thin titanium layer is evaporated on the inner and outer cavity surface, Ti being a stronger getter than Nb. The high-temperature treatment with Ti getter is often called postpurification. The titanium layer is removed afterwards by a 800 μm BCP of the inner surface. A BCP of about 30 μm is applied at the outer surface since the Kapitza resistance of titanium-coated niobium immersed in superfluid helium is about a factor of 2 larger than that of pure niobium [11]. After final heat treatment and BCP the cavities are mechanically tuned to adjust the resonance frequency to the design value and to obtain equal field amplitudes in all 9 cells. This is followed by a slight BCP, three steps of high-pressure water rinsing (100 bar), and drying in a class 10 clean room. As a last step, the rf test is performed in a superfluid helium bath cryostat.

A severe drawback of the postpurification is the considerable grain growth accompanied by a softening of the niobium. Postpurified-treated cavities are quite vulnerable to plastic deformation and have to be handled with great care.

V. RESULTS ON CAVITY PERFORMANCE AND QUALITY CONTROL MEASURES

A. Overview

Figure 12 shows the excitation curve of the best 9-cell resonator measured so far; plotted is the quality factor[12] Q_0 as a function of the accelerating electric field E_{acc}. An
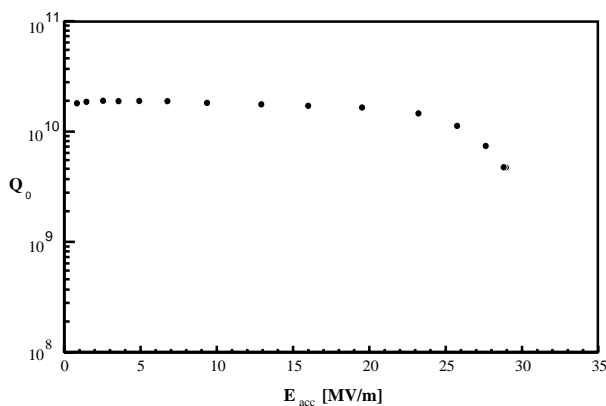
FIG. 12. Excitation curve of the best TESLA 9-cell cavity measured to date. The cavity was cooled by superfluid helium of 2 K.

[12]The quality factor is defined as $Q_0 = f/\Delta f$, where f is the resonance frequency and Δf is the full width at half height of the resonance curve of the "unloaded" cavity.

almost constant and high value of 2×10^{10} is observed up to 25 MV/m.

The importance of various cavity treatment steps for arriving at such a good performance is illustrated in the next figure. A strong degradation is usually observed if a foreign particle is sticking on the cavity surface, leading either to field emission of electrons or to local overheating in the rf field. At Cornell University an *in situ* method for destroying field emitters was invented [23], called "high power processing," which in many cases can improve the high-field capability; see Fig. 13(a). Removal of field-emitting particles by high-pressure water rinsing, a technique developed at CERN [24], may dramatically improve the excitation curve [Fig. 13(b)]. The beneficial effect of a 1400 °C heat treatment, first tried out at Cornell [25] and Saclay [26], is seen in Fig. 13(c). Finally, an incomplete removal of the titanium surface layer in the BCP following the 1400 °C heat treatment may strongly limit the attainable gradient. Here additional BCP is advantageous [Fig. 13(d)].

B. Results from the first series of TTF cavities

After the successful test of two prototype 9-cell resonators, a total of 27 cavities equipped with main power and HOM coupler flanges were ordered at four European companies. These cavities were foreseen for installation in the TTF linac with an expected gradient of at least 15 MV/m at $Q_0 > 3 \times 10^9$. However, in the specification given to the companies no guaranteed gradient was required. According to the test results obtained at TTF these resonators can be classified into four categories: (1) 16 cavities without any known material and fabrication defects, or with minor defects which could be repaired; (2) three cavities with serious material defects; (3) six cavities with imperfect equator welds; (4) two cavities with serious fabrication defects (not fully penetrated electron beam welds or with holes burned during welding; these were rejected). One cavity has not yet been tested.

The test results for the cavities of class 1 in a vertical bath cryostat with superfluid helium cooling at 2 K are summarized in Fig. 14. It is seen that the TTF design goal of 15 MV/m is clearly exceeded. Nine of the resonators fulfill even the more stringent specification of TESLA ($E_{\text{acc}} \geq 25$ MV/m at $Q_0 \geq 5 \times 10^9$).

The excitation curves of the class 2 cavities (Fig. 15) are characterized by sudden drops in quality factor with increasing field and rather low maximum gradients.

Temperature mapping revealed spots of excessive heating at isolated spots which were far away from the EB welds. An example is shown in Fig. 16(a). The defective cell was cut from the resonator and subjected to further investigation [27]. An eddy-current scan, performed at the Bundesanstalt für Materialforschung (BAM) in Berlin, showed a pronounced signal at the defect location. With x-ray radiography, also carried out at BAM, a dark spot with
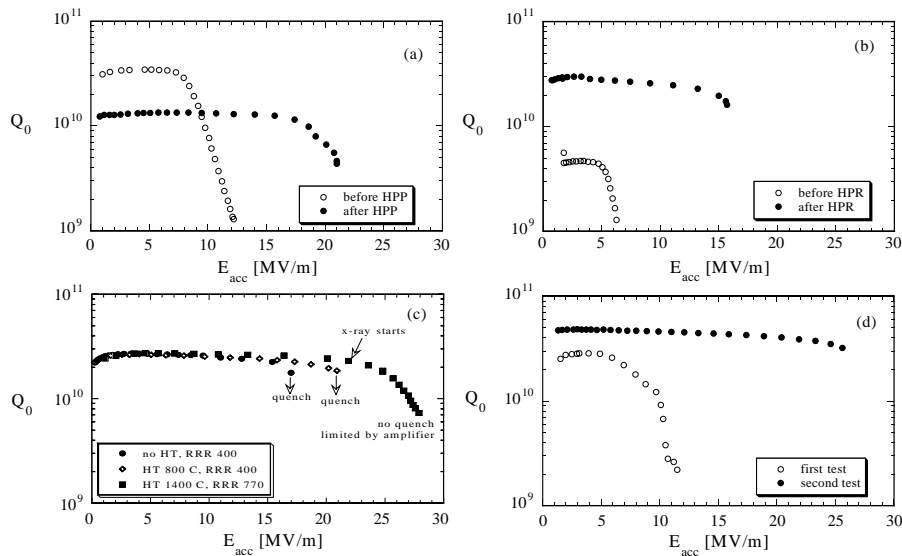
FIG. 13. Improvement in cavity performance due to various treatments: (a) high power processing (HPP), (b) high pressure water rinsing (HPR), (c) successive application of 800 °C and 1400 °C heat treatment (HT), and (d) removal of surface defects or titanium in grain boundaries by additional BCP.

a size of 0.2–0.3 mm was seen [Fig. 16(b)] indicating an inclusion of foreign material with a higher nuclear charge than niobium. Neutron absorption measurements at the Forschungszentrum GKSS in Geesthacht gave no signal, indicating that the neutron absorption coefficient of the unknown contamination was similar to that of Nb. The identification of the foreign inclusion was finally accomplished using x-ray fluorescence at the Hamburger Synchrotron-strahlungslabor (HASYLAB) at DESY. Fluorescence was observed at photon energies corresponding to the characteristic x-ray lines of tantalum $L_1 = 11.682$ keV, $L_2 = 11.136$ keV, and $L_3 = 9.881$ keV.

The synchrotron radiation fluorescence analysis method features sufficient sensitivity to perform a scan of the tantalum contents in the niobium by looking at the lines $TaK_{\alpha 1} = 57.532$ keV, $TaK_{\alpha 2} = 56.277$ keV, and $TaK_{\beta} = 65.223$ keV. The average Ta content in the bulk

Nb was about 200 ppm but rose to 2000 ppm in the spot region. The RRR dropped correspondingly from 330 to about 60.

The six cavities in class 3 were produced by one company and exhibited premature quenches at gradients of 10–14 MV/m and a slope in the $Q(E)$ curve (Fig. 17). Two of the resonators were investigated in greater detail [28]. Temperature mapping revealed strong heating at several spots on the equator weld [Fig. 18(b)]. The temperature rise as a function of the surface magnetic field is plotted in Fig. 18(c) for one sensor position above the weld and three positions on the weld. In the first case a growth proportional to B^2 is observed as expected for a constant surface resistance. On the weld, however, a much stronger rise is seen ranging from B^5 to B^8. This is clear evidence for a contamination of the weld seam.
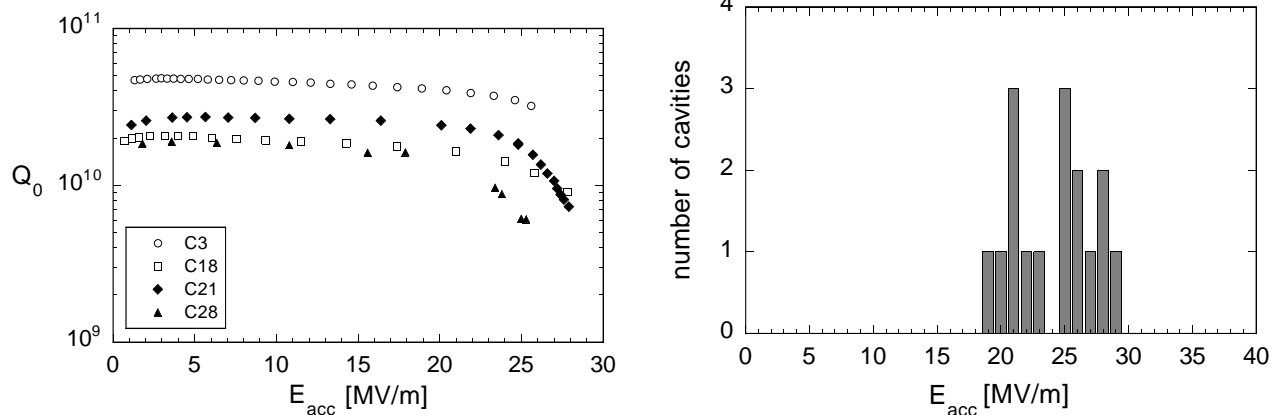

FIG. 14. (a) Excitation curves of the best 9-cell resonator of each of the four manufacturers. (b) Distribution of maximum gradients for the resonators of class 1, requiring a quality factor $Q_0 \geq 5 \times 10^9$.
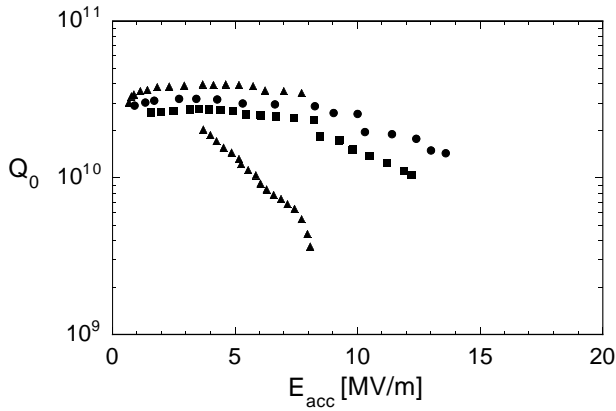
FIG. 15.   Excitation curves of three cavities with serious material defects (class 2). Cavity C5 (▲) exhibited a jump in quality factor.
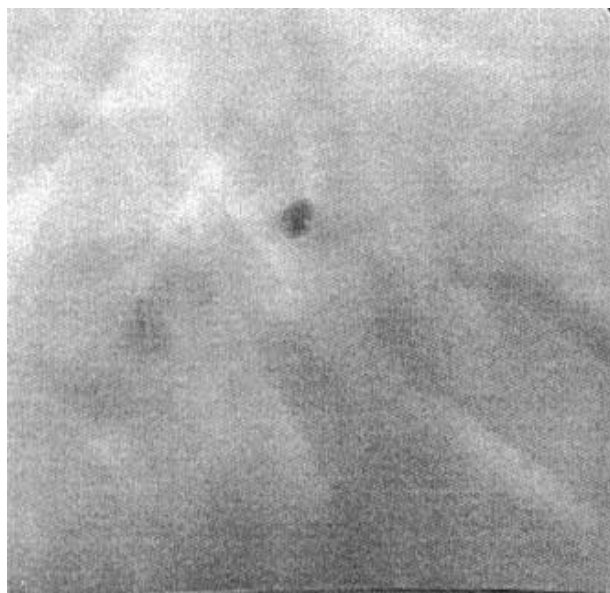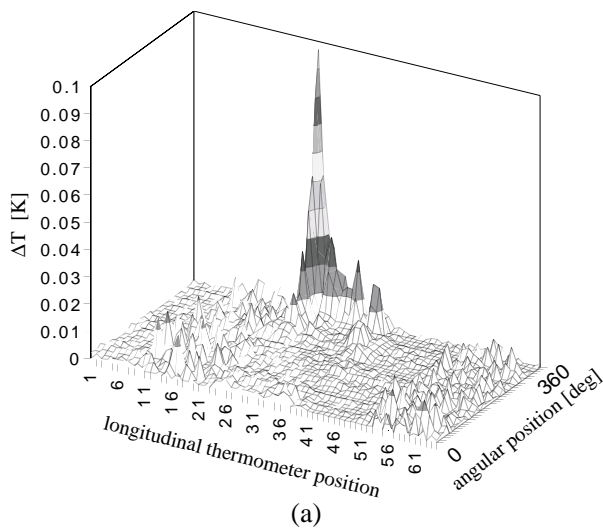

(a)

(b)

FIG. 16.   (a) Temperature map of cell 5 of cavity C6 showing excessive heating at a localized spot. (b) Positive print of an x-ray radiograph showing the "hot spot" as a dark point.

Once the reason for the reduced performance of the cavities in class 3 had been identified, a new 9-cell resonator was manufactured by the same company applying careful preparation steps of the weld region: a 2 μm chemical etching not more than 8 h in advance of the EB welding, rinsing with ultrapure water and drying in a clean room. A rastered electron beam was used for welding with 50% penetration in the first weld layer and 100% in the second. The new cavity indeed showed excellent performance and achieved 24.5 MV/m; see Fig. 17. The same applies for later cavities made by this company.

The average gradient of the cavities without serious material or fabrication defects amounts to 20.1 $\pm$ 6.2 MV/m at $Q_0 = 5 \times 10^9$, where the error represents the rms of the distribution.

C. Diagnostic methods and quality control

The deficiencies encountered in the first series production of TESLA cavities have initiated the development of diagnostic methods and quality control procedures.

1. Electron microscopy

Scanning electron microscopy with energy-dispersive x-ray analysis (EDX) is used to identify foreign elements on the surface. Only a depth of about 1 μm can be penetrated, so one has to remove layer by layer to determine the diffusion depth of titanium or other elements. Alternatively, one can cut the material and scan the cut region. The titanium layer applied in the high temperature treatment has been found to extend to a depth of about 10 μm in the bulk niobium. The sensitivity of the EDX method is rather limited; a Ti fraction below 0.5% is undetectable. Auger electron spectroscopy offers higher sensitivity, and, using this method, titanium migration at grain boundaries has been found to a depth of 50−100 μm. Hence this large
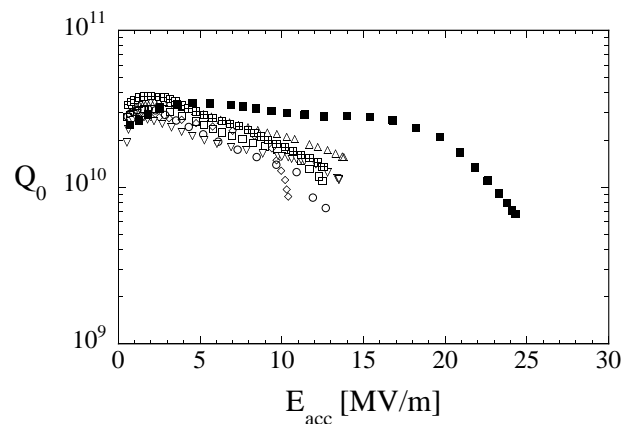

FIG. 17.   Excitation curves of six cavities with imperfect equator welds (class 3). Also shown is a resonator (■) made later by the same company, following stringent cleaning procedures at the equator welds.
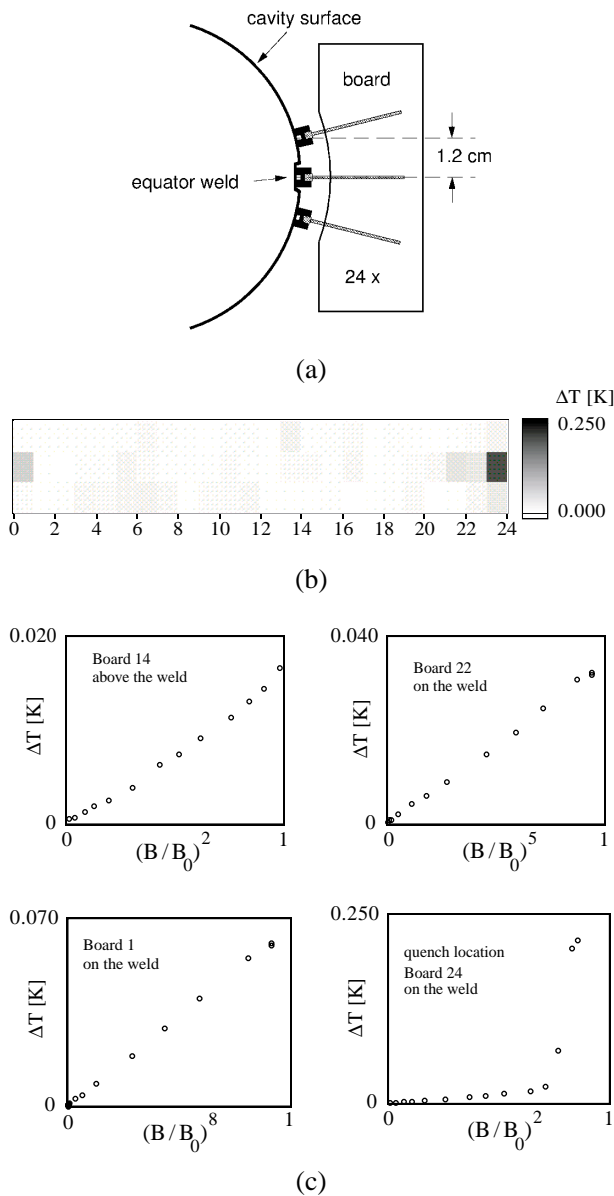
(a)

(b)

(c)

FIG. 18. (a) Location of temperature sensors to determine heating at the equator weld. (b) Temperature map of the equator region from cell 5 of cavity C9 just below the quench. (c) Temperature rise at various locations as a function of $(B/B_0)^n$ with n between 2 and 8 and $B_0 = 50$ mT.

thickness must be removed from the rf surface by BCP after postpurification with a Ti getter. The detrimental effect of insufficient titanium removal has already been shown in Fig. 13(d). The microscopic methods are restricted to small samples and cannot be used to study entire cavities.

2. X-ray fluorescence

The narrow band x-ray beams at HASYLAB permit element identification via fluorescence analysis. In principle the existing apparatus allows the scanning of a whole niobium sheet such as is used for producing a half-cell; however, the procedure would be far too time consuming.

A practical device for the quality control of all niobium sheets going into cavity production is a high-resolution eddy-current system developed by the BAM in Berlin. The apparatus is shown in Fig. 19. The frequency used is
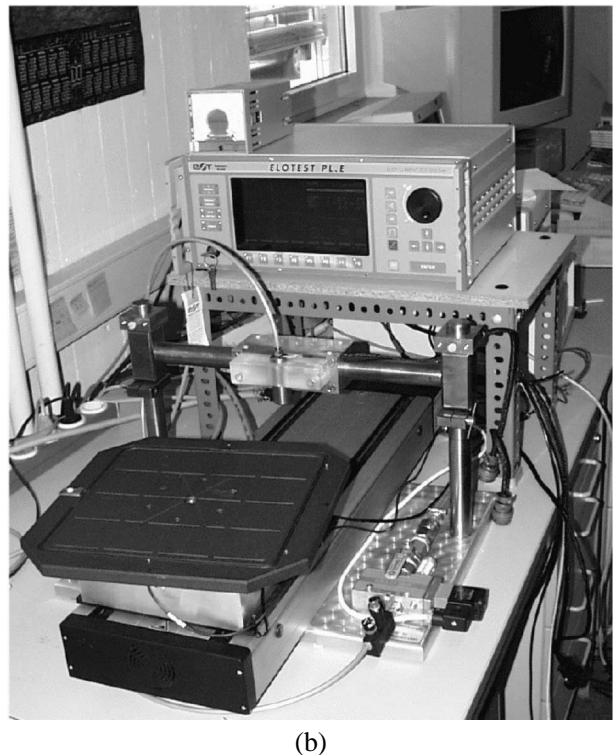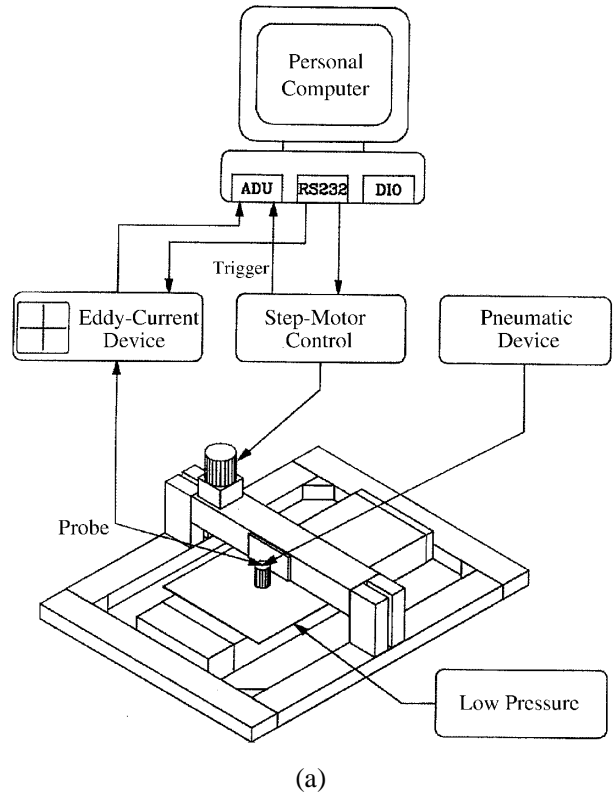

(a)

(b)

FIG. 19. (a) Schematic view of the *xy* eddy-current scanning system. (b) Photograph of the new rotating scanning system.

100 kHz corresponding to a penetration depth of 0.5 mm in niobium at room temperature. The maximum scanning speed is 1 m/s. The scanning probe containing the inducing and receiving coils floats on an air pillow to avoid friction. The machined base plate contains holes for evacuating the space between this plate and the Nb sheet. The atmospheric pressure is sufficient to flatten the 265×265 mm^2 niobium sheets to within 0.1 mm, which is important for a high sensitivity scan. The performance

Ta-Deposit E: ∅=0.2 mm

Ta-Deposit D: ∅=0.2 mm   Ta-Deposit C: ∅=1 mm

Ta-Deposit A: ∅=0.5 mm   Ta-Deposit B: ∅=1 mm
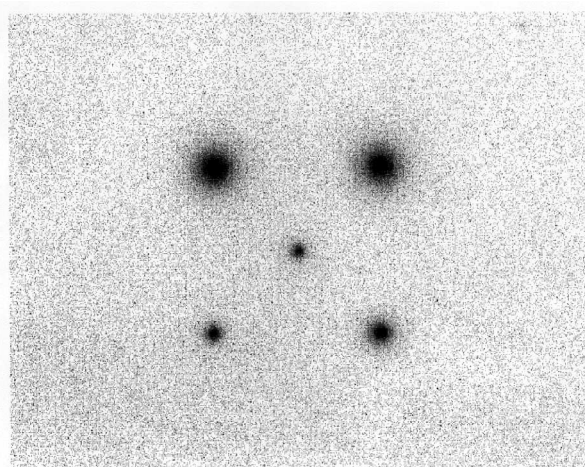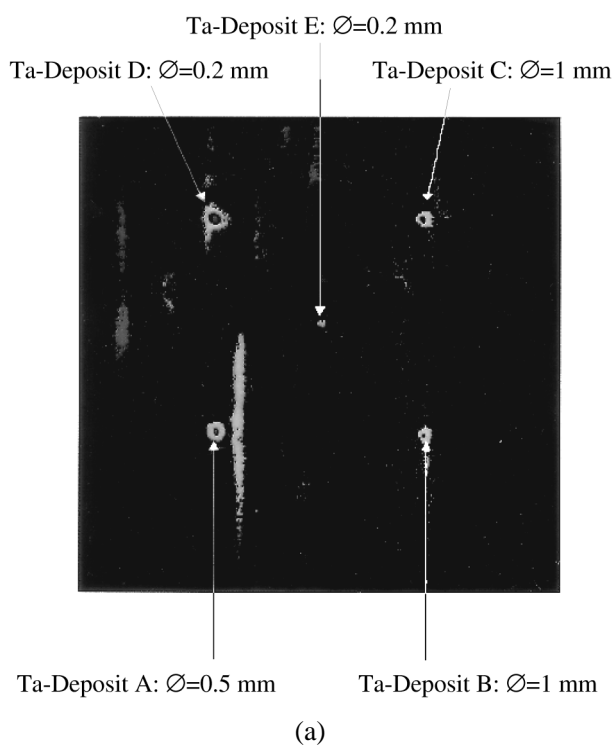
(a)

(b)

FIG. 20. (a) Eddy-current scan of a specially prepared Nb sheet with Ta implantations at 5 locations. The vertical lines are caused by microphonics. (b) Neutron activation analysis of the same sheet.

of the apparatus was tested with a Nb test sheet containing implanted tantalum deposits of 0.2 to 1 mm diameter. The scanned picture [Fig. 20(a)] demonstrates that Ta clusters are clearly visible. Using this eddy-current apparatus the tantalum inclusion in cavity C6 was easily detectable.

In the meantime, an improved eddy-current scanning device has been designed and built at BAM which operates similar to a turntable and allows for much higher scanning speeds and better sensitivity since the accelerations of the probe head occurring in *xy* scans are avoided. A two-frequency principle is applied in the new system. Scanning with high frequency (about 1 MHz) allows detection of surface irregularities while the low frequency test (about 150 kHz) is sensitive to bulk inclusions. The high and low frequency signals are picked up simultaneously. Very high sensitivity is achieved by signal subtraction.

3. Neutron activation analysis

The eddy-current scan allows the detection of foreign materials in the niobium but is not suitable for identification. Neutron activation analysis permits a nondestructive determination of the contaminants provided they have radioactive isotopes with a sufficiently long half-life. Experiments were carried out at the research reactor BER II of the Hahn Meitner Institut in Berlin. The niobium sheets are exposed to a thermal neutron flux of 10^9 cm^{-2} s^{-1} for some 5 h. The radioactive isotope ^{94}Nb has a half-life of 6.2 min while ^{182}Ta has a much longer half-life of 115 days. Two weeks after the irradiation the ^{94}Nb activity has dropped to such a low level that tantalum fractions in the ppm range can be identified. Figure 20(b) shows the implanted tantalum clusters in the specially prepared Nb plate with great clarity. Also, the uniformly dissolved Ta is visible and the inferred concentration of 200 ppm is in agreement with the chemical analysis. The activation analysis is far too time consuming for series checks but can be quite useful in identifying special contaminations found with the eddy-current system. Ten Nb sheets from the regular production were investigated without showing any evidence for tantalum clusters.

D. Present status of TTF cavities

1. Improvements in cavity production

For the second series, 25 cavities have been ordered at four firms. The second production differed from the first one in three main aspects:

(1) Stricter quality control of niobium. The niobium sheets for the second series were all eddy-current scanned to eliminate material with tantalum or other foreign inclusions before the deep drawing of half-cells. From 715 sheets, 637 were found free of defects, 63 showed grinding marks or imprints from rolling, and 15 exhibited large

signals which, in most cases, were due to small iron chips. No further Nb sheets with tantalum inclusions were found. Most of the rejected sheets will be recoverable by applying some chemical etching. The iron inclusions were caused by mechanical wear of the rolls used for sheet rolling. In the meantime new rolls have been installed. The eddy-current check has turned out to be an important quality control not only for the cavity manufacturer but also for the supplier of the niobium sheets.

(2) Weld preparation. Stringent requirements were imposed on the electron-beam welding procedure to prevent the degraded performance at the equator welds encountered in the first series. After mechanical trimming the weld regions were requested to be cleaned by a slight chemical etching, ultrapure water rinsing, and clean room drying not more than 8 h in advance of the EB welding. The success of these two additional quality control measures has been convincing: no foreign material inclusions nor weld contaminations were found in the cavities tested so far.

(3) Replacement of Nb flanges by NbTi flanges. In the first cavity series the flanges at the beam pipes and the coupler ports were made by rolling over the 2 mm thick niobium pipes. The sealing against the stainless steel counter flanges was provided by Helicoflex gaskets. This simple design appeared satisfactory in a number of prototype cavities but proved quite unreliable in the series production, mainly due to a softening of the niobium during the 1400 °C heat treatment. Most of the 9-cell cavities had to be flanged more than once to become leak tight in superfluid helium. This caused not only time delays but also severe problems with contamination and field emission. Therefore an alternative flange design was needed [29]. The material was selected to be EB weldable to niobium and to possess a surface hardness equivalent to that of standard UHV flange material (stainless steel 316 LN/DIN 4429). Niobium-titanium conforms to these requirements at a reasonable cost. Contrary to pure niobium, the alloy NbTi (ratio 45/55 in wt. %) shows no softening after the 1400 °C heat treatment and only a moderate crystal growth. O-ring-type aluminum gaskets provide reliable seals in superfluid helium and are easier to clean than Helicoflex gaskets. During cavity etching the sealing surface must be protected from the acid.

2. Test results in vertical cryostat

All new cavities were subjected to the standard treatment described in Sec. IV B, including the postpurification with titanium getter at 1400 °C. Twenty resonators have been tested to date. Only one rf test was performed for each resonator in the first round. If some limitation was found, the cavity was put aside for further treatment. The results of the first test sequence are summarized in Fig. 21. It is seen that eight cavities reach or exceed the TESLA specification of $E_{acc} \geq 25$ MV/m with a quality
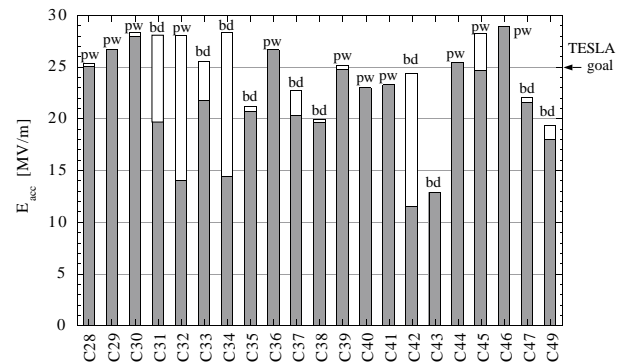

FIG. 21. Test results of the second cavity series (crosshatched bars); plotted is the highest gradient achieved in the first rf test of each cavity at $Q_0 \geq 5 \times 10^9$. Cavities with poor initial performance were subjected to an additional BCP and high pressure water rinsing and tested again (open bars). Field limitation by amplifier power (pw) or thermal breakdown (bd) is indicated for the best gradient.

factor above 5×10^9. Eight cavities are in the range of 18 to 23 MV/m while four cavities show a much lower performance. In cavity C43 a hole was burned during equator welding which was repaired by welding in a niobium plug; the cavity quenched at 13 MV/m at exactly this position. It is rather unlikely that C43 can be recovered by repeating the repair. Therefore, in future cavity production repaired holes in EB welds will no longer be acceptable. The cavities C32, C34, and C42 showed very strong field emission in the first test. They have been improved in the meantime by additional BCP and high pressure water rinsing; see Fig. 21. Excluding the defective cavity C43, the average gradient is 25.0 ± 3.2 MV/m at $Q_0 = 5 \times 10^9$.

3. Tests with main power coupler in horizontal cryostat

After the successful test in the vertical bath cryostat the cavities are welded into their liquid helium container and equipped with the main power coupler. The external Q is typically 2×10^6, while in the vertical test an input antenna with an external Q of more than 10^{11} is used. Four cavities of the first production series and 13 of the second series have been tested together with their main power coupler in a horizontal cryostat. The accelerating fields achieved in the vertical and horizontal test are quite similar, as shown in Fig. 22. In a few cases, reduced performance was seen due to field emission while several cavities improved their field capability due to the fact that with the main power coupler pulsed operation is possible instead of the cw operation in the vertical cryostat. These results indicate that the good performance of the cavities can indeed be preserved after assembly of the liquid helium container and the power coupler provided extreme care is taken to avoid foreign particles from entering the cavity during these assembly steps.
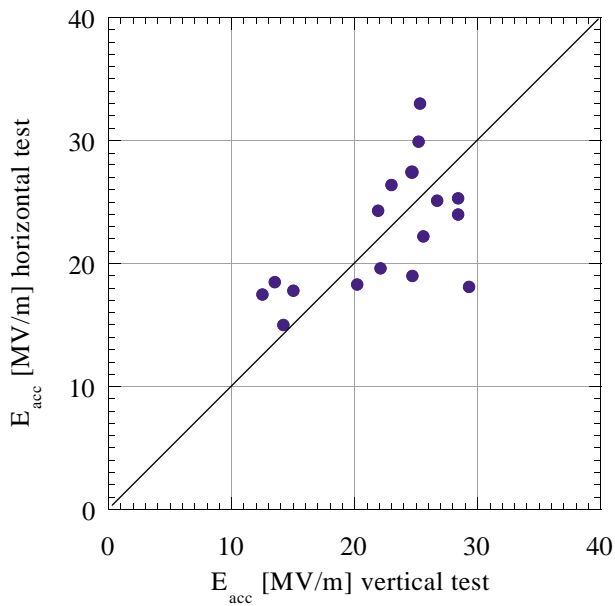
FIG. 22. Comparison of vertical and horizontal test results. The average accelerating field achieved in the vertical test with cw excitation is 22.3 MV/m, in the horizontal test with pulsed excitation 22.5 MV/m. Most of these cavities are from the second production.

4. Cavity improvement by heat treatment

The beneficial effect of the 800 °C and 1400 °C heat treatments has been shown in Fig. 13(c). Ten of the 9-cell cavities have been tested after the intermediate 800 °C step yielding an average gradient of 20.7 MV/m. The 1400 °C treatment with titanium getter raised the average gradient to 24.4 MV/m. It should be noted that part of the 3.7 MV/m improvement may be due to the additional etching of about 80 μm. An interesting correlation is obtained by plotting the maximum gradient as a function of the measured RRR of the cavity; see Fig. 23. This figure clearly indicates that a higher heat conductivity leads to higher accelerating fields, at least if the standard BCP treatment is applied to prepare the cavity surface.
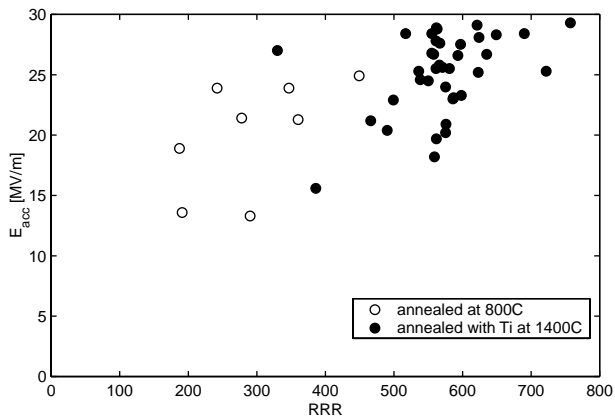

FIG. 23. Maximum gradient as a function of RRR.

VI. RF CONTROL SYSTEM AND PERFORMANCE OF THE CAVITIES WITH ELECTRON BEAM

A. General demands on the rf control system

The requirements on the stability of the accelerating field in a superconducting acceleration structure are comparable to those in a normal-conducting cavity. However, the nature and magnitude of the perturbations to be controlled are rather different. Superconducting cavities possess a very narrow bandwidth and are therefore highly susceptible to mechanical perturbations. Significant phase and amplitude errors are induced by the resulting frequency variations. Perturbations can be excited by mechanical vibrations (microphonics), changes in helium pressure and level, or Lorentz forces. Slow changes in frequency, on the time scale of minutes or longer, are corrected by a frequency tuner, while faster changes are counteracted by an amplitude and phase modulation of the incident rf power.

The demands on amplitude and phase stability of the TESLA Test Facility cavities are driven by the maximum tolerable energy spread in the TTF linac. The design goal is a relative spread of $\sigma_E/E = 2 \times 10^{-3}$ implying a gradient and phase stability of the order of 1×10^{-3} and 1.6°, respectively. For cost reasons, up to 32 cavities will be powered by a single klystron. Hence it is not possible to control individual cavities but only the vector sum of the field vectors in these 32 cavities.

One constraint to be observed is that the rf power needed for control should be minimized. The rf control system must also be robust against variations of system parameters such as beam loading and klystron gain.

The pulsed structure of the rf power and the beam at TTF, shown in Fig 24, puts demanding requirements on the rf control system. Amplitude and phase control is obviously needed during the flattop of 800 μs when the beam is accelerated, but it is equally desirable to control the field during cavity filling to ensure proper beam injection
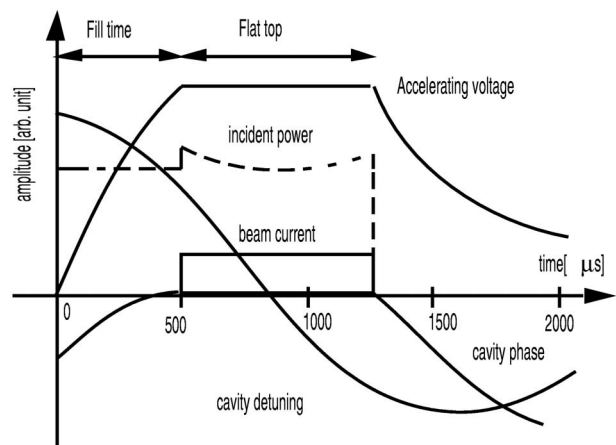

FIG. 24. Pulse structure of TTF cavity operation. Shown are accelerating voltage with 500 μs filling time and 800 μs flattop, incident power, beam current, cavity phase, and cavity detuning.

conditions. Field control is aggravated by the transients induced by the subpicosecond electron bunches which have a repetition rate of 1 to 9 MHz.

For a detailed discussion of the basic principles of rf systems used in superconducting electron linacs and their operational performance, refer to Refs. [30,31].

B. Sources of field perturbations

There are two basic mechanisms which influence the magnitude and phase of the accelerating field in a super-conducting cavity: (i) variations in klystron power or beam loading (bunch charge) and (ii) modulation of the cavity resonance frequency.

Perturbations of the accelerating field through time-varying field excitations are dominated by changes in beam loading. One must distinguish between transients caused by the pulsed structure of the beam current and stochastic fluctuations of the bunch charge. The transients caused by the regular bunch train in the TTF linac (800 sub-picosecond bunches of 8 nC each, spaced by 1 μs) are of the order of 1% per 10 μs; the typical bunch charge fluc-tuations of 10% induce field fluctuations of about 1%. In both cases the effect of the fast source fluctuations on the cavity field is diminished by the long time constant of the cavity.[13]

Mechanical changes of the shape and eigenfrequency of the cavities caused by microphonics are a source of ampli-tude and phase jitter which has bothered superconducting accelerator technology throughout its development. In the TTF cavities the sensitivity of the resonance frequency to a longitudinal deformation is about 300 Hz/μm. Heavy machinery can transmit vibrations through the ground, the support, and the cryostat to the cavity. Vacuum pumps can interact with the cavity through the beam tubes, and the compressors and pumps of the refrigerator may generate mechanical vibrations which travel along the He trans-fer line into the cryostat. Also, helium pressure varia-tions lead to changes in resonance frequency, as shown in Fig. 25(a). The rms frequency spread due to micro-phonics, measured in 16 cavities, is 9.5 $\pm$ 5.3 Hz and is thus surprisingly small for a superconducting cavity system [see Fig. 25(b)].

At high accelerating gradients the Lorentz forces become a severe perturbation. The corresponding frequency shift is proportional to the square of the ac-celerating field according to $\Delta f = -KE_{\text{acc}}^2$ with $K \approx$ 1 Hz(MV^{-1} m^{-1})^2. Figure 26(a) shows a cw measure-ment of the resonance curve with a strong distortion

---

[13]The cavity with power coupler is adjusted to an external Q of 3×10^6 at 25 MV/m, corresponding to a time constant of about 700 μs. The consequence is a low-pass filter characteristic.
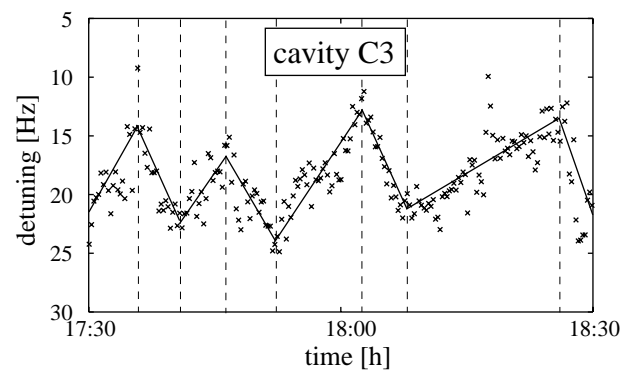

(a)
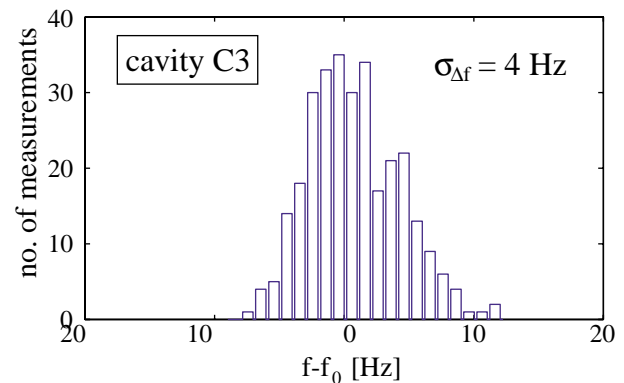
(b)

FIG. 25. Fluctuations of the cavity resonance frequency. (a) Slow drifts caused by helium pressure variations. The sensitivity is 10 Hz/mbar. (b) Random variations of resonance frequency after correction for the slow drift.

caused by Lorentz forces. In cw operation the frequency shift can be easily corrected for by mechanical tuning. In the pulsed mode employed at the TTF linac this is not possible since the mechanical tuner is far too slow. Hence a time-dependent detuning is unavoidable. In order to keep the deviation from the nominal resonance frequency within acceptable limits the cavities are predetuned before filling. The measured dynamic detuning of cavity C39 during the 1.3 ms long rf pulse is shown in Fig. 26(b) for accelerating fields of 15 to 30 MV/m. Choosing a predetuning of +300 Hz, the eigenfrequency at 25 MV/m changes dynamically from +100 to −120 Hz during the 800 μs duration of the beam pulse.

In steady state (cw) operation, at a gradient of 25 MV/m and a beam current of 8 mA, a klystron power of 210 kW is required per 9-cell cavity. In pulsed mode ≈15% additional rf power is needed to maintain a constant accel-erating gradient in the presence of cavity detuning. The frequency changes from microphonics and helium pressure fluctuations lead to comparable extra power requirements. The klystron should be operated 10% below saturation to guarantee sufficient gain in the feed-back loop.
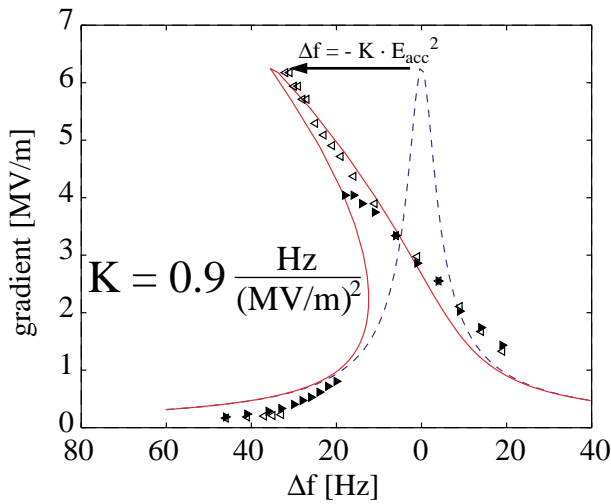
(b)
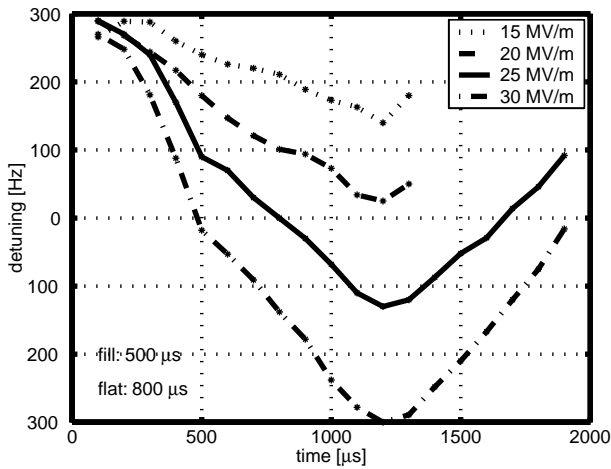
(b)

FIG. 26. (Color) (a) Influence of Lorentz forces on the shape of the resonance curve of a sc cavity in cw operation. The left part of the curve was mapped out by approaching the resonance from below, the right part by coming from above. (b) Dynamical detuning of cavity C39 during the TESLA pulse. In pulsed operation the resonance is approached from above.

C. rf control design considerations

The amplitude and phase errors from Lorentz force detuning, beam transients, and microphonics are of the order of 5% and 20°, respectively. These errors must be suppressed by 1–2 orders of magnitude. Fortunately, the dominant errors are repetitive (Lorentz forces and beam transients) and can be largely eliminated by means of a feedforward compensation. It should be noted, however, that bunch-to-bunch fluctuations of the beam current cannot be suppressed by the rf control system since the gain bandwidth product is limited to about 1 MHz due to the low-pass characteristics of the cavity, the bandwidth limitations of electronics and klystrons, and cable delay.

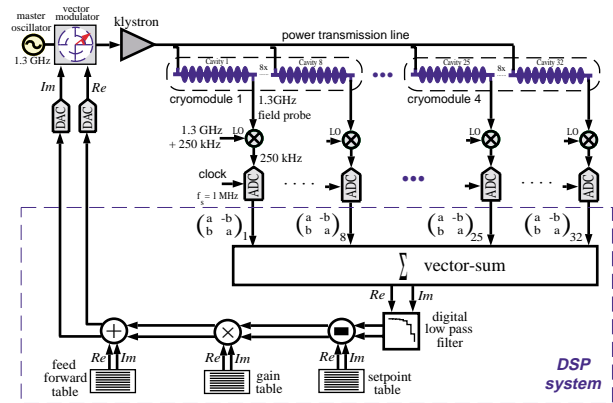Fast amplitude and phase control can be accomplished by modulation of the incident rf wave which is common

FIG. 27. (Color) Schematic of the digital rf control system.

to 32 cavities. The control of an individual cavity field is not possible. The layout of the TTF digital rf control system is shown in Fig. 27. The vector modulator for the incident wave is designed as a so-called "I/Q modulator" controlling the real and imaginary parts of the complex cavity field vector instead of amplitude and phase. This has the advantage that the coupling between the two feedback loops is minimized and the problem of large phase uncertainties at small amplitude is avoided.

The detectors for cavity field, incident, and reflected wave are implemented as digital detectors for the real and imaginary parts. The rf signals are converted to an intermediate frequency of 250 kHz and sampled at a rate of 1 MHz, which means that two subsequent data points yield the real and the imaginary parts of the cavity field vectors. These vectors are multiplied with 2×2 rotation matrices to correct for phase offsets and to calibrate the gradients of the individual cavity probe signals. The vector sum is calculated and a Kalman filter is applied which provides an optimal state (cavity field) estimate by correcting for delays in the feedback loop and by taking stochastic sensor and process noise into account. Finally, the nominal set point is subtracted and a time-optimal gain matrix is applied to calculate the new actuator setting (the Re and Im control inputs to the vector modulator). Adaptive feedforward is realized by means of a table containing the systematic variations, thereby reducing the task of the feedback loop to control the remaining stochastic fluctuations. The feedforward tables are continuously updated to take care of slow changes in parameters such as average detuning angle, microphonic noise level, and phase shift in the feedforward path.

D. Operational experience

The major purpose of the TESLA Test Facility linac is to demonstrate that all major accelerator subsystems meet the technical and operational requirements of the TESLA collider. Currently the TTF linac is equipped with two cryomodules each containing eight cavities. The cavities

are routinely operated at the design gradient of TTF of 15 MV/m, providing a beam energy of 260 MeV.

An important prerequisite of the proper functioning of the vector-sum control of 16 to 32 cavities is an equal response of the field pickup probes in the individual cavities. A first step is to adjust the phase of the incident rf wave to the same value in all cavities by means of three-stub tuners in the waveguides. Secondly, the transients induced by the bunched beam are used to obtain a relative calibration of the pickup probes, in terms of both amplitude and phase. Typical data taken at the initial start-up of a linac run are shown in Fig. 28. Ideally the lengths of the field vectors should all be identical since the signals are induced by the same electron bunch in all cavities. The observed length differences indicate a variation in the coupling of the pickup antenna to the beam-induced cavity field, which has to be corrected. The different phase angles of the field vectors are mainly due to different signal delays. The complex field vectors are rotated by matrix multiplication in digital signal processors to yield all zero phase. Moreover they are normalized to the same amplitude to correct for the different couplings of the pickup antennas to the cavity fields. Once this calibration has been performed the vector sum of the 16 or 32 cavities is a meaningful measure of the total accelerating voltage supplied to the beam. The calibration is verified with a measurement of the beam energy in a magnetic spectrometer.

The required amplitude stability of 1×10^{-3} and phase stability of $\sigma_\phi \leq 1.6°$ can be achieved during most of the
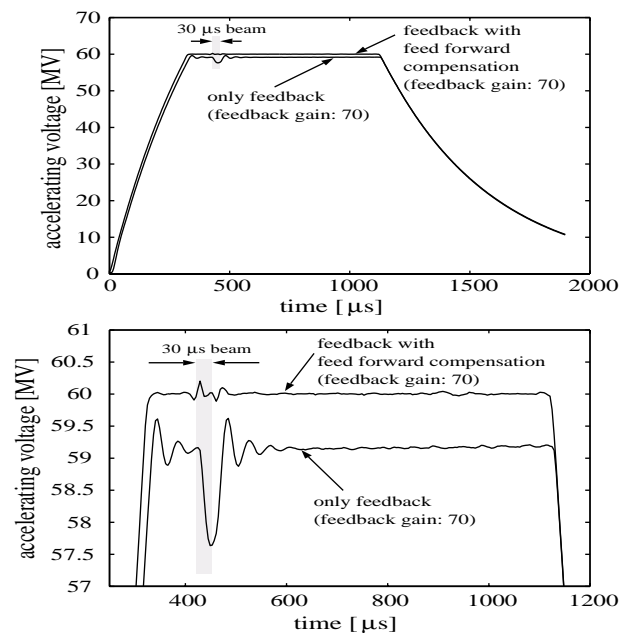
FIG. 29. Field regulation of the vector sum of eight cavities without and with adaptive feedforward. The lower graph shows an enlarged view of the plateau region.

beam pulse duration with the exception of the beam transient induced when turning on the beam. Without feedback the transient of a 30 μs beam pulse at 8 mA would be of the order of 1 MV/m. This transient can be reduced to about 0.2 MV/m by turning on feedback. The effectiveness of the feedback system is limited by the loop delay of 5 μs and the unity-gain bandwidth of about 20 kHz. The 0.2 MV/m transient is repetitive with a high degree of reproducibility. Using feedforward it can be further suppressed by more than 1 order of magnitude, as shown in Fig. 29. Slow drifts are corrected for by making the feedforward system adaptive [32]. The feedforward tables are updated on a time scale of minutes.

VII. CAVITIES OF HIGHER GRADIENTS

Both the TESLA collider and the x-ray FEL would profit from the development of cavities which can reach higher accelerating fields (i.e., higher particle energies) and higher quality factors (i.e., reduced operating costs of the accelerators). The TESLA design energy of 250 GeV per beam requires a gradient of 25 MV/m in the present 9-cell cavities. The results shown in Sec. V D demonstrate that TESLA could indeed be realized with a moderate improvement in the present cavity fabrication and preparation methods. However, for particle physics an energy upgrade of the collider would be of highest interest, and hence there is a strong motivation to push the field capability of the cavities closer to the physical limit of about 50 MV/m, which is determined by the superheating field of niobium. There are three main reasons that the theoretical limit has not yet
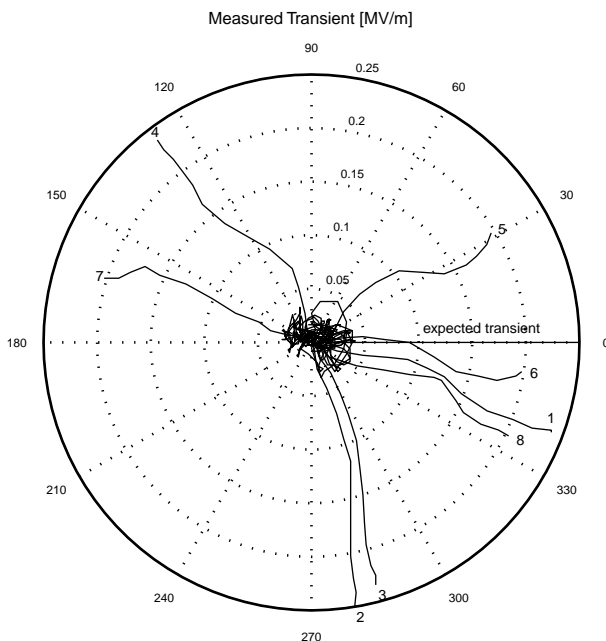

FIG. 28. Beam induced transients (cavity field vectors) obtained by measuring the cavity fields with and without beam pulses. The noise in the signals can be estimated from the erratic motion at the center of the plot. This region represents the first 50 μs of the measurement before the arrival of the beam pulse.

been attained in multicell resonators: (1) foreign material contamination in the niobium, (2) insufficient quality and cleanliness of the inner rf surface, and (3) insufficient mechanical stability of the resonators. An R&D program has been initiated aiming at improvements in all three directions. Furthermore, the feasibility of seamless cavities is being investigated.

A. Quality improvement of niobium

Niobium for microwave resonators has to be of high purity for several reasons: (i) dissolved gases such as hydrogen, oxygen, and nitrogen reduce the heat conductivity at liquid helium temperature and degrade the cooling of the rf surface; (ii) contamination by foreign metals may lead to magnetic flux pinning and heat dissipation in rf fields; (iii) normal-conducting or weakly superconducting clusters close to the rf surface are particularly dangerous . The Nb ingots contain about 500 ppm of finely dispersed tantalum. It appears unlikely that the Ta clusters found in some early TTF cavities might have been caused by this "natural" Ta content. Rather there is some suspicion that Ta grains might have dropped into the Nb melt during the various remeltings of the Nb ingot in an electron-beam melting furnace because such furnaces are often used for Ta production as well. To avoid contamination by foreign metals, a dedicated electron-beam melting furnace would appear highly desirable but seems to be too cost intensive in the present R&D phase of TESLA. Also, more stringent requirements on the quality of the furnace vacuum (lower pressure, absence of hydrocarbons) would improve the Nb purity. The production steps following the EB melting (machining, forging, and sheet rolling of the ingot) may also introduce dirt. The corresponding facilities need careful inspection and probably some upgrading. The present TTF cavities have been made from niobium with gas contents in the few ppm range and an RRR of 300. Ten 9-cell cavities have been measured after both 800 °C and 1400 °C firings. The average gain in gradient was about 4 MV/m. It would be highly desirable to eliminate the tedious and costly 1400 °C heat treatment of complete cavities. One possibility might be to produce a niobium ingot with an RRR of more than 500. This is presently not our favored approach, mainly for cost reasons.

For the present R&D program, the main emphasis is on the production of ingots with RRR $\geq$ 300, but with improved quality by starting from niobium raw material with reduced foreign material content, especially tantalum well below 500 ppm. Stricter quality assurance during machining, forging, and sheet rolling should prevent metal flakes or other foreign material from being pressed into the niobium surface deeper than a few μm. To increase the RRR from 300 to about 600, it is planned to study the technical feasibility[14] of a 1400 °C heat treatment at the

dumbbell stage (2 half-cells joined by a weld at the iris). This procedure would be preferable compared to the heat treatment of whole cavities which must be carefully supported in a Nb frame to prevent plastic deformation, while such a precaution is not needed for dumbbells. However, there is a strong incentive to find cavity treatment methods which would permit elimination of the 1400 °C heat treatment altogether. According to the results obtained at KEK [33], electropolishing seems to offer this chance (see below).

B. Improvement in cavity fabrication and preparation

Once half-cells or dumbbells of high RRR have been produced, it is then mandatory to perform the electron-beam welding of the cavities in a vacuum of a few times 10^{-6} mbar in order to avoid degradation of the RRR in the welds. The EB welding machines available at industrial companies achieve vacua of only 5×10^{-5} mbar and are hence inadequate for this purpose. An EB welding machine at CERN is equipped with a much better vacuum system. This EB apparatus is being used for a single-cell test program. For the future cavity improvement program a new electron-beam welding apparatus will be installed at DESY with a state-of-the-art electron gun, allowing computer-controlled beam manipulations, and an oil-free vacuum chamber fulfilling UHV standards.

The industrially produced cavities undergo an elaborate treatment at TTF before they can be installed in the accelerator. A 150–200 μm thick damage layer is removed from the rf surface because otherwise gradients of 25 MV/m appear inaccessible. As explained in Sec. IV, the present method is BCP which leads to a rather rough surface with strong etching in the grain boundaries. An alternative method is "electropolishing" (EP) in which the material is removed in an acid mixture under current flow. Sharp edges and burrs are smoothed out and a very glossy surface can be obtained. For a number of years remarkable results have been obtained at KEK with electropolishing of 1-cell niobium cavities. Recently, a collaboration between KEK and Saclay has convincingly demonstrated that EP raises the accelerating field by more than 7 MV/m with respect to BCP. Several 1-cell cavities from Saclay, which already showed good performance after the standard BCP, exhibited a clear gain after the application of EP [34]. Conversely, an electropolished cavity which had reached 37 MV/m suffered a degradation after subsequent BCP. These results are a strong indication that electropolishing is the superior treatment method.

---

[14]At Cornell University cavities have been successfully fabricated from RRR = 1000 material. Likewise, the TTF cavity C19 was made from postpurified half-cells and showed good performance.
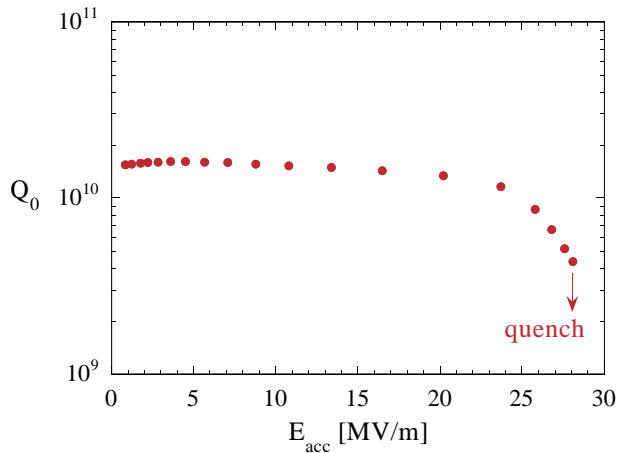
FIG. 30. (Color) Excitation curve of a TESLA 9-cell cavity showing a drop of quality factor without any field emission.

CERN, DESY, KEK, and Saclay started a joint R&D program with electropolishing of half-cells and 1-cell cavities in August, 1998. Recent test results yield gradients around 40 MV/m [35] and hence the same good performance as was achieved at KEK. The transfer of the EP technology to 9-cell resonators requires considerable effort. It is planned to do this in collaboration with industry.

Recently it has been found [36] that an essential prerequisite for achieving gradients in the 40 MV/m regime is a baking at 100 °C to 150 °C for up to 48 h while the cavity is evacuated, after the final high-pressure water rinsing. In electropolished cavities this procedure removes the drop of quality factor towards high gradients which is often observed without any indication of field emission. Such a drop is usually also found in chemically etched cavities; see, for example, Fig. 30. Experiments at Saclay [37] have shown that a baking may improve the $Q(E)$ curve; however, part of the Q reduction at high field may be due to local magnetic field enhancements at the sharp grain boundaries of BCP treated cavities [38].

C. Mechanical stability of the cavities

The stiffening rings joining neighboring cells in the TESLA resonator are adequate to limit Lorentz-force detuning up to accelerating fields of 25 MV/m. Beyond 25 MV/m the cavity reinforcement provided by these rings is insufficient. Hence, an alternative stiffening scheme must be developed for cavities in the 35–40 MV/m regime. A promising approach has been taken at Orsay and Saclay. The basic idea is to reinforce a thin-walled niobium cavity by a 2 mm thick copper layer which is plasma sprayed onto the outer wall. Several successful tests have been made [39]. The copper plating has a potential danger since Nb and Cu have rather different thermal contractions. The deformation of a cavity upon cooldown and the resulting frequency shift need investigation. Another phenomenon has been observed

in cavities made from explosion-bonded niobium-copper sheets: when these cavities were quenched, a reduction in quality factor Q_0 was observed [40]. An explanation may be trapped magnetic flux from thermoelectric currents at the copper-niobium interface. It is unknown whether this undesirable effect happens also in copper-sprayed cavities. An alternative to copper spraying might be the reinforcement of a niobium cavity by depositing some sort of metallic "foam," using the plasma or high velocity spraying technique. If the layer is porous, the superfluid helium penetrating the voids should provide ample cooling.

The cavity reinforcement by plasma or high-velocity spraying appears to be a promising approach, but considerable R&D work needs to be done to decide whether this is a viable technique for the TESLA cavities.

D. Seamless cavities

The EB welds in the present resonator design are a potential risk. Great care has to be taken to avoid holes, craters, or contamination in the welds which usually have a detrimental effect on the high-field capability. A cavity without weld connections in the regions of high electric or magnetic rf field would certainly be less vulnerable to small mistakes during fabrication. For this reason the TESLA Collaboration decided several years ago to investigate the feasibility of producing seamless cavities. Two routes have been followed: spinning and hydroforming.

At the Legnaro National Laboratory of INFN in Italy, the spinning technique [41] has been successfully applied to form cavities out of niobium sheets. The next step will be to produce a larger quantity of 1-cell, 3-cell, and, finally, 9-cell cavities from seamless Nb tubes with an RRR of 300. In the cavities spun from flat sheets a very high degree of material deformation was needed, leading to a rough inner cavity surface. Gradients between 25 and 32 MV/m were obtained after grinding and heavy etching (removal of more than 500 μm) [42]. Starting from a tube, the amount of deformation will be much less and a smoother inner surface can be expected. This R&D effort is well underway and the first resonators can be expected in early 2000.

The hydroforming of cavities from seamless niobium tubes is being pursued at DESY [43]. Despite initial hydroforming difficulties, related to inhomogeneous mechanical properties of the niobium tubes, four single cell cavities have been successfully built so far. Three of these were tested and reached accelerating fields of 23 to 27 MV/m. In a very recent test[15] 32.5 MV/m was achieved at $Q_0 = 2 \times 10^{10}$. Most remarkable is the fact

---

[15]Preparation and testing of the hydroformed cavities were carried out by P. Kneisel at Jefferson Laboratory, Newport News, Virginia.

that the cavity was produced from low RRR niobium (RRR = 100). It received a 1400 °C heat treatment raising the RRR to 300–400. The surface was prepared by grinding and 250 μm BCP.

E. Niobium sputtered cavities

Recent investigations at CERN [14] and Saclay [44] show that single-cell copper cavities with a niobium sputter layer of about 1 μm thickness are able to reach accelerating fields beyond 20 MV/m. These results appear so promising that CERN and DESY have agreed to initiate an R&D program on 1.3 GHz single-cell sputtered cavities aiming at gradients in the 30 MV/m regime and quality factors above 5×10^9. High-performance sputtered cavities would certainly be of utmost interest for the TESLA project for cost reasons. Another advantage would be the suppression of Lorentz force detuning by choosing a sufficiently thick copper wall.

F. The superstructure concept

The present TTF cavities are equipped with one main power coupler and two higher order mode couplers per 9-cell resonator. The length of the interconnection between two cavities has been set to $3\lambda/2$ ($\lambda = 0.23$ m is the rf wavelength) in order to suppress cavity-to-cavity coupling of the accelerating mode. A shortening of the interconnection is made possible by the "superstructure" concept, devised by Sekutowicz [45]. Four 7-cell cavities of TESLA geometry are joined by beam pipes of length $\lambda/2$. The pipe diameter is increased to permit an energy flow from one cavity to the next, hence one main power coupler is sufficient to feed the entire superstructure. One HOM coupler per short beam pipe section provides sufficient damping of dangerous higher modes in both neighboring cavities. Each 7-cell cavity will be equipped with its own LHe vessel and frequency tuner. Therefore, in the superstructure the field homogeneity tuning (equal field amplitude in all cells) and the HOM damping can be handled at the subunit level. The main advantages of the superstructure are an increase in the active acceleration length in TESLA—the design energy of 250 GeV per beam can be reached with a gradient of 22 MV/m—and a savings in rf components, especially power couplers.

A copper model of the superstructure is presently used to verify the theoretically predicted performance. This model allows individual cell tuning, field profile adjustment, investigation of transients in selected cells, test of the HOM damping scheme, and measurement of the cavity couplings to the fundamental mode coupler. Also, the influence of mechanical tolerances is studied. First results are promising [46]. A niobium superstructure prototype is under construction and will be tested with beam in the TTF linac in early 2001.

[1] *Proceedings of the 1st TESLA Workshop, 1990,* edited by H. Padamsee (Cornell University Report No. CLNS-90-1029, 1990).

[2] TESLA-Report 95-01, 1995.

[3] C. Reece *et al.,* in *Proceedings of the 1995 Particle Accelerator Conference and International Conference on High Energy Accelerators, Dallas, Texas* (IEEE, Piscataway, NJ, 1995), p. 1512.

[4] DESY 1997-048, ECFA 1997-182, 1997.

[5] G. Müller, in *Proceedings of the 3rd Workshop on rf Superconductivity, Argonne, Illinois, 1988,* edited by K. W. Shepard (ANL, Argonne, IL, 1988), p. 331.

[6] B. Bonin, in *Proceedings of the CERN Accelerator School, Hamburg, 1995,* edited by S. Turner (CERN, Geneva, 1996), p. 191.

[7] W. Weingarten, in *Proceedings of the CERN Accelerator School, Hamburg, 1995* (Ref. [6]), p. 167.

[8] T. Schilcher, DESY Report No. TESLA 95-12, 1995.

[9] B. Bonin, Supercond. Sci. Technology **9**, 453 (1996).

[10] K. Schulze, J. Met. **33**, 33 (1981).

[11] A. Boucheffa *et al.,* in *Proceedings of the 7th Workshop on rf Superconductivity, Gif-sur-Yvette, France, 1995,* edited by B. Bonin (CEA, Saclay, 1996), p. 659.

[12] J. Matricon and D. Saint-James, Phys. Lett. **24A**, 241 (1967).

[13] T. Hays *et al.,* in *Proceedings of the 7th Workshop on rf Superconductivity, Gif-sur-Yvette, France, 1995* (Ref. [11]), p. 437.

[14] C. Benvenuti *et al.,* in Proceedings of the 9th Workshop on rf Superconductivity, Santa Fe, 1999 (to be published).

[15] R. H. Fowler and L. Nordheim, Proc. R. Soc. London A **119**, 173 (1928); Math. Phys. Sci. **119**, 173 (1928).

[16] H. Padamsee, J. Knobloch, and T. Hays, *RF Superconductivity for Accelerators* (Wiley, New York, 1998).

[17] H. Padamsee, in *Proceedings of the 5th Workshop on Superconductivity, Hamburg, Germany, 1991,* edited by D. Proch (DESY, Hamburg, 1992), p. 963.

[18] U. Lauströer *et al.,* DESY Report No. DESY M-87-03, 1987.

[19] A. W. Chao and M. Tigner, *Handbook of Accelerator Physics and Engineering* (World Scientific, Singapore, 1999).

[20] W. Albach and G. A. Voss, Z. Angew. Phys. **9**, 111 (1957).

[21] W. D. Möller, in Proceedings of the 9th Workshop on rf Superconductivity, Santa Fe, New Mexico, 1999 (Ref. [14]).

[22] J. Tückmantel, in *Proceedings of the 1995 Particle Accelerator Conference and International Conference on High Energy Accelerators, Dallas, 1995* (Ref. [3]), p. 1642.

[23] J. Graber, Nucl. Instrum. Methods Phys. Res., Sect. A **350**, 572 (1994).

[24] P. Bernard *et al.,* in *Proceedings of the Third European Particle Accelerator Conference, Berlin, 1992,* edited by E. Henke, H. Homeyer, and Ch. Petit-Jean-Genaz (Frontíeres, Gif-sur-Yvette, 1992), p. 1269.

[25] H. Padamsee *et al.,* in *Proceedings of the 4th Workshop on rf Superconductivity, Tsukuba, Japan, 1989,* edited by Y. Kojima (KEK, Ibaraki, 1990), p. 207.

[26] H. Safa *et al.,* in *Proceedings of the 7th Workshop on rf Superconductivity, Gif-sur-Yvette, France, 1995* (Ref. [11]), p. 649.

[27] W. Singer, D. Proch, and A. Brinkmann, in *Proceedings of the 8th Workshop on rf Superconductivity, Abano Terme, Italy, 1997,* edited by V. Palmieri and A. Lombardi (LNL-INFN, Padova, 1998), p. 850.

[28] A. Brinkmann *et al.,* in *Proceedings of the 8th Workshop on rf Superconductivity, Abano Terme, Italy, 1997* (Ref. [27]), p. 452.

[29] K. Zapfe-Düren *et al.,* in *Proceedings of the 8th Workshop on rf Superconductivity, Abano Terme, Italy, 1997* (Ref. [27]), p. 457.

[30] H.-D. Gräf, in *Proceedings of the 5th Workshop on rf Superconductivity, Hamburg, Germany, 1991* (Ref. [17]), p. 317.

[31] S. Simrock, in *Proceedings of the 6th Workshop on rf Superconductivity, Newport News, Virginia, 1993,* edited by R. M. Sundelin (CEBAF, Newport News, 1994), p. 294.

[32] M. Liepe and S. Simrock, in *Proceedings of the 1998 European Particle Accelerator Conference, Stockholm, Sweden,* edited by S. Myers, L. Liljeby, Ch. Petit-Jean-Genaz, J. Poole, and K.-G. Rensfelt (Institute of Physics, Bristol, UK, 1998), p. 1735.

[33] K. Saito, in Proceedings of the 9th Workshop on rf Superconductivity, Santa Fe, New Mexico, 1999 (Ref. [14]).

[34] E. Kako *et al.,* in Proceedings of the 9th Workshop on rf Superconductivity, Santa Fe, 1999 (Ref. [14]).

[35] L. Lilje *et al.,* in Proceedings of the 9th Workshop on rf Superconductivity, Santa Fe, 1999 (Ref. [14]).

[36] P. Kneisel, in Proceedings of the 9th Workshop on rf Superconductivity, Santa Fe, 1999 (Ref. [14]).

[37] P. Charrier *et al.,* in *Proceedings of the 1998 European Particle Accelerator Conference, Stockholm, Sweden* (Ref. [32]), p. 1735.

[38] J. Knobloch *et al.,* in Proceedings of the 9th Workshop on rf Superconductivity, Santa Fe, 1999 (Ref. [14]).

[39] S. Bousson, in Proceedings of the 9th Workshop on rf Superconductivity, Santa Fe, 1999 (Ref. [14]).

[40] T. Fujino *et al.,* in Proceedings of the 9th Workshop on rf Superconductivity, Santa Fe, 1999 (Ref. [14]).

[41] V. Palmieri, in *Proceedings of the 8th Workshop on rf Superconductivity, Abano Terme, Italy, 1997* (Ref. [27]).

[42] P. Kneisel, V. Palmieri, and K. Saito, in Proceedings of the 9th Workshop on rf Superconductivity, Santa Fe, 1999 (Ref. [14]).

[43] I. Gonin *et al.,* in Proceedings of the 9th Workshop on rf Superconductivity, Santa Fe, 1999 (Ref. [14]).

[44] P. Bosland, A. Aspart, E. Jacques, and M. Ribeaudeau, IEEE Trans. Appl. Supercond **9**, 896 (1999).

[45] J. Sekutowicz, M. Ferrario, and Ch. Tang, Phys. Rev. ST Accel. Beams **2**, 062001 (1999).

[46] H. Chen *et al.,* in Proceedings of the 9th Workshop on rf Superconductivity, Santa Fe, 1999 (Ref. [14]).